Clin Exp Metastasis
DOI 10.1007/s10585-012-9506-0

RESEARCH PAPER

Dipyridamole prevents triple-negative breast-cancer progression

Daniela Spano · Jean-Claude Marshall · Natascia Marino · Daniela De Martino · Alessia Romano · Maria Nunzia Scoppettuolo · Anna Maria Bello · Valeria Di Dato · Luigi Navas · Gennaro De Vita · Chiara Medaglia · Patricia S. Steeg · Massimo Zollo

Received: 27 January 2012 / Accepted: 13 June 2012

Abstract Dipyridamole is a widely prescribed drug in ischemic disorders, and it is here investigated for potential clinical use as a new treatment for breast cancer. Xenograft mice bearing triple-negative breast cancer 4T1-Luc or MDA-MB-231T cells were generated. In these in vivo models, dipyridamole effects were investigated for primary tumor growth, metastasis formation, cell cycle, apoptosis, signaling pathways, immune cell infiltration, and serum inflammatory cytokines levels. Dipyridamole significantly reduced primary tumor growth and metastasis formation by intraperitoneal administration. Treatment with 15 mg/kg/day dipyridamole reduced mean primary tumor size by 67.5 % ($p = 0.0433$), while treatment with 30 mg/kg/day dipyridamole resulted in an almost a total reduction in primary tumors ($p = 0.0182$). Experimental metastasis assays show dipyridamole reduces metastasis formation by 47.5 % in the MDA-MB-231T xenograft model ($p = 0.0122$), and by 50.26 % in the 4T1-Luc xenograft model ($p = 0.0292$). In vivo dipyridamole decreased activated β-catenin by 38.64 % ($p < 0.0001$), phospho-ERK1/2 by 25.05 % ($p = 0.0129$), phospho-p65 by 67.82 % ($p < 0.0001$) and doubled the expression of IkBα ($p = 0.0019$), thus revealing significant effects on Wnt, ERK1/2-MAPK and NF-kB pathways in both animal models. Moreover dipyridamole significantly decreased the infiltration of tumor-associated macrophages and myeloid-derived suppressor cells in primary tumors ($p < 0.005$), and the inflammatory cytokines levels in the sera of the treated mice. We suggest that when used at appropriate doses and with the correct mode of administration, dipyridamole is a promising agent for breast-cancer treatment, thus also implying its potential use in other cancers that show those highly activated pathways.

Keywords Dipyridamole · Metastasis · ERK1/2-MAPK · Wnt · NF-kB · Immune cell infiltration · Tumor microenvironment

Abbreviations

AGP	α_1 Acid glycoprotein
BCRP/ABCG2	Human breast cancer resistance protein
BLI	Bioluminescence imaging
CI	Cell index
DMEM	Dulbecco's modified Eagle's medium

Daniela De Martino, Alessia Romano and Maria Nunzia Scoppettuolo contributed equally to the work.

Electronic supplementary material The online version of this article (doi:10.1007/s10585-012-9506-0) contains supplementary material, which is available to authorized users.

D. Spano · N. Marino · D. De Martino · M. N. Scoppettuolo · A. M. Bello · V. Di Dato · L. Navas · G. De Vita · C. Medaglia · M. Zollo (✉)
Centro di Ingegneria Genetica (CEINGE) Biotecnologie Avanzate, Via Gaetano Salvatore 486, 80145 Naples, Italy
e-mail: zollo@ceinge.unina.it; massimo.zollo@unina.it

D. Spano · D. De Martino · A. Romano · M. N. Scoppettuolo · A. M. Bello · V. Di Dato · G. De Vita · C. Medaglia · M. Zollo
Dipartimento di Biochimica e Biotecnologie Mediche, 'Federico II' University of Naples, Via Sergio Pansini 5, 80131 Naples, Italy

J.-C. Marshall · N. Marino · P. S. Steeg
Women's Cancers Section, Laboratory of Molecular Pharmacology, National Cancer Institute, 37 Convent Drive, Bethesda, MD 20892, USA

L. Navas
Dipartimento di Scienze Cliniche Veterinarie, Sezione di Clinica Chirurgica, 'Federico II' University of Naples, Via Delpino, 1, 80137 Naples, Italy

Published online: 04 July 2012

DMSO	Dimethylsulfoxide
G-CSF	Granulocyte colony-stimulating factor
GM-CSF	Granulocyte-macrophage colony-stimulating factor
IHC	Immunohistochemistry
IL-1α	Interleukin-1α
IL-1β	Interleukin-1β
MCP-1	Monocyte chemotactic protein 1
MDSCs	Myeloid-derived suppressor cells
MIP-1a	Macrophage inflammatory protein 1a
MMP9	Matrix metalloproteinase 9
MTS	(3-(4,5-dimethylthiazol-2-yl)-5-(3-carboxymethoxyphenyl)-2-(4-sulfophenyl)-2H-tetrazolium)
PBS	Phosphate-buffered saline
PEG	Polyethylene glycol
PGK	Phosphoglucokinase
RTCA	Real-time cell analysis
RT-CES	Real-time cell electronic sensor
SCF	Stem cell factor
SE	Standard error
SEM	Standard error of the mean
TAMs	Tumor-associated macrophages

Introduction

Despite many advances in the treatment of breast cancer, worldwide, over 450,000 women die annually of this disease [1], with tumor metastasis the major cause of these deaths [2]. Therefore, agents that can prevent metastatic colonization of breast tumor cells represent an essential advance in the therapeutics of this disease. Herein, we identify a novel role for dipyridamole, a drug already approved by the US Food and Drug Administration and the European Union, as an inhibitor of breast-cancer progression.

Dipyridamole is a potent competitive inhibitor of equilibrative nucleoside transport [3]. The salvage of extracellular nucleosides and nucleobases via this transport system results in repletion of the nucleotide pools [4] and constitutes one of a number of mechanisms by which tumors resist antimetabolite drugs [5]. Several studies have shown that in vitro, dipyridamole can significantly increase the cytotoxic and antitumor activities of a variety of chemotherapeutic agents [6–12]. The underlying mechanism here is both prevention of nucleoside and nucleobase salvage, and an increase in the intracellular accumulation of the toxic metabolites [6, 10–14]. Dipyridamole has also been shown to enhance in vitro TRAIL tumoricidal activity [15]. Furthermore, it is an effective inhibitor of the human breast-cancer-resistance protein BCRP/ABCG2 [16], which is a drug efflux transporter, and which confers resistance to a large number of chemotherapeutic agents by enhancing the drug efflux [17].

Most importantly, the relationship between dipyridamole and cancer is further emphasized by the anti-platelet aggregation property of dipyridamole [18]. Due to these properties, dipyridamole is currently used in the clinic in combination with aspirin as a vasodilator for ischemic disorders [19]. To date, there is evidence for a contribution of platelets in metastasis formation. Platelets are known to interact with tumor cells to form aggregates, which can enhance tumor-cell arrest in the vasculature, thus releasing growth factors and preventing immune attack [20]. Based on these observations it is not surprising that anti-coagulants and agents that interfere with platelet aggregation, such as anti-thrombins, can prevent tumor metastases [21].

The clinic potential of dipyridamole for the treatment of metastasis in human cancers has been tested previously in combination with several cytotoxic drugs [22–24]. Furthermore, recently, the clinic exploitation of dipyridamole in combination with perifosine for metastasis treatment in breast-cancer xenograft animal models has been investigated [25, 26]. These studies, in which dipyridamole was used in combination with cytotoxic drugs, make the evaluation of the clinic potential of dipyridamole for cancer treatment more difficult.

We have here investigated the potential role of dipyridamole as a single agent in the prevention of tumorigenesis and metastasis in multiple models of triple-negative (estrogen and progesterone receptor-negative, Her-2 normal) breast cancers, a subtype that has few effective therapies [27]. Our findings provide evidence that intraperitoneal administration of dipyridamole impairs primary tumor growth and metastasis in breast-cancer xenograft animal models. Moreover, our data identify new mechanisms of action of dipyridamole, which is shown to inhibit the ERK1/2-MAPK, NF-kB and Wnt signaling pathways, and to prevent the accumulation of inflammatory cells in the tumor microenvironment. These data suggest that this safe, already approved agent might have a new use in appropriately designed clinical trials.

Materials and methods

Drug preparation

Persantin® Retard modified-release capsules containing 200 mg dipyridamole (B01AC07; Boehringer Ingelheim) were dissolved at 6 mM concentration in PBS-PEG (phosphate-buffered saline-polyethylene glycol 400 (Sigma)) (v/v) or in dimethylsulfoxide (DMSO). After dipyridamole was dissolved in PBS-PEG, the solution was sterilized by

passing it through a 0.22 μm filter. The dipyridamole solution in DMSO was used in the proliferation assays in real-time using the xCelligence system. In all of the other experiments the dipyridamole solution in PBS-PEG was used.

Cell culture

Triple-negative murine 4T1-Luc and human MDA-MB-231T breast-cancer cell lines were used for the in vitro and in vivo experiments. 4T1-Luc cells were used for in vivo implantation into the mammary fat pad and for metastasis experiments. MDA-MB-231T cells were used for in vivo lung-metastasis experiments. HEK293T cells were used for the luciferase reporter assay. All of these cells were grown in high-glucose Dulbecco's modified Eagle's medium (DMEM; Invitrogen) supplemented with 10 % (v/v) fetal bovine serum (Invitrogen), 2 mM L-glutamine (Invitrogen), and 1 % (v/v) antibiotics (10000 U/ml penicillin, 10 mg/ml streptomycin [Invitrogen]). The cells were grown at 37 °C in a humidified atmosphere of 95 % air, 5 % CO_2 (v/v).

Proliferation assay

Proliferation assays were performed using the CellTiter 96 Aqueous One Solution Cell Proliferation Assay (Promega). The 4T1-Luc cells (2×10^3/well) and MDA-MB-231T cells (3×10^3/well) were plated into 96-well plates and treated with PBS-PEG (control) or PBS-PEG containing 10, 50 or 100 μM dipyridamole, for 0, 24, 48 and 72 h. Each experimental point was assessed in quadruplicate. The medium supplemented with PBS-PEG or dipyridamole was replaced twice daily. For each experimental point, 20 μl (3-(4,5-dimethylthiazol-2-yl)-5-(3-carboxymethoxyphenyl)-2-(4-sulfophenyl)-2H-tetrazolium) (MTS) solution (1.90 mg/ml) was added to each well, and the cells were incubated for 2 h at 37 °C. Absorbance was then measured at 490 nm using a microtitre plate reader (VICTOR^3 1420 Multilabel Counter, Perkin Elmer). For each experimental point, the means of absorbance and their standard errors (SE) were calculated. A total of two independent sets of experiments were performed.

Flow cytometry

The 4T1-Luc and MDA-MB-231T cells were treated with PBS-PEG (control) or dipyridamole (10, 50, 100 μM) for 24 h. The medium supplemented with PBS-PEG or dipyridamole was replaced twice daily.

For the cell-cycle analysis, after treatment, the cells were resuspended in PBS containing 0.002 % Nonidet P40, 12.5 μg/ml ribonuclease A, and 20 μg/ml propidium iodide, incubated at room temperature for 3 h in the dark, and analyzed on a FACScan flow cytometer (Becton–Dickinson Immunocytometry Systems). For each experimental point, the cell-cycle analysis was performed in triplicate. For each experimental point, the means of percent cell population in cell cycle phases ±SE were calculated. Two independent sets of experiments were performed.

For the evaluation of the percentages of Annexin-V-positive cells, after 24 h treatment, 2×10^5 4T1-Luc and MDA-MB-231T cells were incubated for 30 min with a FITC-conjugated anti-Annexin V antibody (BD Pharmingen) and analyzed using a BD FACSCanto II flow cytometer (BD Biosciences, Oxford, UK). The collected data were analyzed using the FACSDiva software, version 6 (BD Biosciences). Each experimental point was assessed in duplicate. For each experimental point, the means of percent cell population ±SE were calculated. Two independent sets of experiments were performed.

For the evaluation of the percentages of CD49f$^+$ cells, after treatment, 2×10^5 4T1-Luc cells were incubated for 30 min with a FITC-conjugated anti-CD49f antibody (BD Pharmingen) and analyzed using a BD FACSAria flow cytometer (BD Biosciences, Oxford, UK). The collected data were analyzed using the FACSDiva software, version 6 (BD Biosciences). Each experimental point was assessed in duplicate. For each experimental point, the means of percent CD49f$^+$ cell population ±SE were calculated. Two independent sets of experiments were performed.

Caspase-3 activity assay

The 4T1-Luc cells were treated with PBS-PEG (control) or dipyridamole (10, 50, 100 μM) for 24 h. The medium supplemented with PBS-PEG or dipyridamole was replaced twice daily. After the treatment, the cells were lysed in RIPA buffer (50 mM Tris–HCl, pH 8.0, 150 mM NaCl, 1 % Triton X-100, 10 % glycerol) in the presence of protease (Roche) and phosphatase (1 mM $NaVO_3$, 50 mM NaF) inhibitors. Then, 100 μg total protein extract was assessed in a reaction mix containing 20 mM PIPES, pH 7.2, 100 mM NaCl, 10 mM DTT, 1 mM EDTA, 0.1 % (w/v) CHAPS, 10 % (w/v) sucrose, and 40 μM Ac-DEVD-AFC, the caspase-3 fluorogenic substrate (BD Pharmingen). Each experimental point was assessed in triplicate. The reaction mixes were incubated for 1 h at 37 °C. Absorbance was measured at 490 nm using a microtiter plate reader (VICTOR^3 1420 Multilabel Counter, Perkin Elmer). For each experimental point, the mean absorbances ±SE were calculated. A total of two independent sets of experiments were performed.

Cell migration assays

The effects of dipyridamole on cell migration were analyzed by using chamber inserts (24-well format, polycarbonate membrane filter, 8 μm pore size; Corning). Here, 2.5×10^4 4T1-Luc cells or 1×10^5 MDA-MB-231T cells were seeded into the upper chamber in DMEM without fetal bovine serum, in the presence of PBS-PEG (control) or dipyridamole (10, 50, 100 μM). The DMEM in the lower chamber contained fetal bovine serum (5 % for 4T1-Luc cells, 10 % for MDA-MB-231T cells), which served as the chemoattractant; this was also supplemented with PBS-PEG or dipyridamole (10, 50, 100 μM). After a 4 h incubation at 37 °C, the cells migrating to the lower membrane surface were fixed and stained with hematoxylin/eosin. The 4T1-Luc cells were counted per membrane under a light microscope. The MDA-MB-231T cells were photographed and counted in three random fields per membrane at 10× magnification under a light microscope. Each experimental point was in duplicate, and two independent sets of experiments were carried out. For each experimental point, the mean ± SE of the number of migrated cells per membrane/field were calculated.

xCelligence system

The Real-Time Cell Analysis (RTCA) Instrument developed by Roche uses an xCelligence system that is based on the Real-Time Cell Electronic Sensor (RT-CES) system, which allows label-free dynamic monitoring of cell proliferation and viability in real-time [28]. The electronic readout of impedence is expressed as arbitrary units and called the cell index (CI) [28]. The cell culture conditions on the sensor device were the same as those described above. Proliferation assays in real-time were performed as previously described [28]. Here, 8×10^3 4T1-Luc cells/well or 2×10^4 MDA-MB-231T cells/well were plated into each sensor well of an E-plate 16 (ACEA Biosciences, Inc). Four replicates for each experimental point were used. After the DMSO (control) or dipyridamole addition, the CI was automatically and continuously monitored every 5 min for up to 54 h. For each experimental point, the mean ± standard deviation (SD) of CI were calculated. A total of two independent sets of experiments were performed.

Immunoblotting

Total protein extracts from cells and tumor tissues were prepared and used for immunoblotting, as previously described [29], using the following antibodies: rabbit anti-phospho-p44/42 MAPK (ERK1/2) (Thr 202/Tyr 204) (1:500; Cell Signaling Technology), rabbit anti-ERK1/2 (1:500; Santa Cruz Biotechnology), rabbit anti-phospho-IkB-α (Ser 32/36) (1:200; Santa Cruz Biotechnology), rabbit anti-IkBα (1:3000; Abcam), rabbit anti-phospho-NF-kB p65 (Ser 311) (1:200; Santa Cruz Biotechnology), rabbit anti-NF-kB p65 (1:3000; Abcam), mouse anti-AKT1 (1:500; Cell Signaling Technology), rabbit anti-phospho-AKT (Ser 473) (1:500; Cell Signaling Technology), mouse anti-GSK-3β (1:500; BD Biosciences), rabbit anti-phospho-GSK-3β (Ser 9) (1:500; Cell Signaling Technology), mouse anti-activated β-catenin (1:500; Millipore), mouse anti-β-catenin (1:500; BD Transduction Laboratories), rabbit anti-cyclin D1 (1:250; Cell Signaling Technology), rabbit anti-Survivin (1:500; Abcam) and mouse anti-c-Myc (1:500; Santa Cruz Biotechnology). These antibodies were detected using horseradish peroxidase–conjugated anti-mouse (1:5000; Amersham) and anti-rabbit (1:3000; Amersham) antibodies. A mouse anti-β-actin antibody (1:5000; Sigma-Aldrich) was used as a control for equal loading. Semiquantitative analyses of proteins expression were performed. The bands were quantified by densitometry to obtain an integral optical density (OD) value, which then was normalized with respect to the β-actin value. Then the phospho-protein/protein ratios were determined. For each experimental point, the means of phospho-protein/protein ratios ±SE were calculated.

Luciferase reporter assay

The HEK293T cells were seeded into 96-well plates at a density of 1.35×10^4 cells/well and grown for 24 h. To assess the dipyridamole induced-impairment of β-catenin transcription activity, the cells were then transfected using $CaCl_2$ and 2 × HBS reagent (50 mM HEPES, 280 mM NaCl, 1.5 mM Na_2HPO_4, pH 7) with 15 ng Tk-Renilla luciferase plasmid, 65 ng β-catenin-cmyc-pCAN plasmid, or its empty vector as control, and 25 ng of a firefly luciferase reporter construct, as either: TOP-FLASH, containing four Tcf consensus binding sites upstream of firefly luciferase cDNA; or FOP-FLASH, a plamid with mutated Tcf binding sites; or their empty vector (pGL3) as control (gift from Thomas Clevers) [30] (Upstate Biotechnology). To assess the dipyridamole induced-impairment of NF-kB p65 transcription activity, the cells were then transfected using $CaCl_2$ and 2 × HBS reagent with 15 ng Tk-Renilla luciferase plasmid, 65 ng p65 plasmid, or its empty vector (pcDNA3.1) as control, and 25 ng of a firefly luciferase reporter construct containing the immunoglobulin promoter (IgLuc), or its empty vector (pGL3) as control. After 24 h, the cells were incubated overnight with PBS-PEG (control) or dipyridamole (10, 100 μM) at 37 °C. After this incubation, the total cell lysates were extracted using reporter lysis buffer (Promega), and the luciferase activities were determined using the Dual-Glo Luciferase® Assay System

(Promega) with a microplate Luminometer (Perkin Elmer, EnVision 2102 Multilabel Reader). Firefly luciferase activity was normalized for transfection efficiency by Renilla luciferase activity. Each experimental point was assessed in triplicate. For each experimental point, the means of normalized luciferase activity ±SE were calculated. Two independent sets of experiments were performed.

Quantitative real-time polymerase chain reaction (qRT-PCR)

Total RNA was isolated from cells using Trizol reagent (Invitrogen) according to the manufacturer protocol. After measurement of RNA yield and quality using a NanoDrop machine (Celbio), the cDNA was synthesized by random hexamers with iScript cDNA synthesis kits (Bio-Rad), according to the protocols supplied by Bio-Rad. After digestion with DNAse RNAse-free, two micrograms of total RNA in 20 µl was used in each reaction. qRT-PCR was performed using the SYBR Green PCR Master Mix (Applied Biosystems) and the Applied Biosystems Model 7900HT sequence detection system, according to the protocols supplied by Applied Biosystems. The primers were designed with the Primer Express 2.1 program (Applied Biosystems). All qRT-PCRs were performed in duplicate, with 70 ng ss-cDNA used in each 10-µl reaction. β-actin mRNA was used to normalize the mRNA concentrations. The primer sequences for the tested genes were the following:

m-p27 forward, 5′-CTTCCGCCTGCAGAAATCTC-3′;
m-p27 reverse, 5′-CCATATCCCGGCAGTGCTT-3′;
m-matrix metalloproteinase 9 (MMP9) forward, 5′-TACCCGCTGTATAGCTACCTCGA-3′;
m-MMP9 reverse, GCCACGACCATACAGATACTGGA;
m-phosphoglucokinase (PGK) forward, 5′-GCATCAAATTCTGCTTGGACAATGGA-3′;
m-phosphoglucokinase (PGK) reverse, 5′-CTCTACATGAAAGCGGAGGTTTTCC-3′;
m-β-actin forward, 5′-AGGCCAACCGTGAAAAGATG-3′;
m-β-actin reverse, 5′-GCCTGGATGGCTACGTACATG-3′;
h-p27 forward, 5′- CTGCAGGAACCTCTTCGGC-3′;
h-p27 reverse, 5′- GCTCGCCTCTTCCATGTCTCT-3′;
h-β-actin forward, 5′-GACCCAGATCATGTTTGAGACCTT;
h-β-actin reverse, 5′-CCAGAGGCGTACAGGGATAGC-3′.

For statistical analysis of the gene expression data, the mean fold change $= 2^{-(\text{average } \Delta\Delta Ct)} \pm$ SEM was calculated using the mean difference in the ΔCt between the genes and the internal control. The ΔCt was calculated using the differences in the mean Ct between the genes and the internal control.

In vivo mouse experiments

Athymic nude and Balb/c mice were purchased from Harlan. All of the animal experiments were conducted according to Italian law and under a National Cancer Institute approved Animal Use Agreement. Every effort was made to minimize the suffering of the animals, and to minimize the number of animals used. Seven-week-old mice were anesthetized with 3 % avertin (Sigma) solution, and then had 4T1-Luc cells either implanted into the VIII right-side mammary gland or injected into the left ventricle of the heart. The MDA-MB-231T cells were injected into the tail vein of 7-week-old athymic nude mice. The 4T1-Luc xenograft mice were treated with vehicle (PBS-PEG) or dipyridamole (15, 30, 60 mg/kg/day), for 5 days/week (2 injections/day) for 2–4 weeks, beginning one or two weeks after implantation/injection. The MDA-MB-231T xenograft mice were treated with vehicle (PBS-PEG) or 30 mg/kg/day dipyridamole (2 injections/day) for 6 days/week for 6 weeks, beginning one day after injection. The treatments were administered intraperitoneally or by oral gavage. At the end of the experiments, the primary tumors and the metastatic lungs were dissected out and embedded in paraffin, for immunohistochemistry (IHC) analyses.

In vivo bioluminescence imaging

Cell implantation and tumor growth were monitored by bioluminescence imaging (BLI) acquisition using an IVIS 3D Illumina Imaging System (Xenogen/Caliper). Briefly, the mice were anesthetized with isoflurane, injected intraperitoneally with D-luciferin solution (15 mg/ml stock; 100 µl per 10 g body weight), and imaged. For the intracardiac-injected mice, two acquisitions (ventral and dorsal) were made per mouse; while for the mammary fat-pad implanted mice, one acquisition (ventral) was made per mouse. To quantify the bioluminescence, the integrated fluxes of photons (photons per s) within each area of interest were determined using the Living Images Software Package 3.2 (Xenogen-Caliper). For each intracardiac-injected mouse, the ventral and dorsal integrated fluxes of photons were added together. According to the time and treatment, the mean ± SE of the photon integrated fluxes were calculated for each experimental point.

Lung metastases detection

The MDA-MB-231T breast cancer xenograft mice were sacrificed on day 45 of PBS-PEG or dipyridamole

treatment, and their lungs were removed and infused with Bouin's solution. After fixing in Bouin's solution for 48 h, the number of macroscopically visible metastases on the lung surface was quantified. The tissues were embedded in paraffin for IHC analysis.

Immunohistochemistry

Paraffin sections (7 μm thick) of the tumor specimens were incubated overnight at 4 °C with the following antibodies: rabbit anti-Ki67 (1:100; Abcam), rabbit anti-cleaved caspase-3 (1:500; Cell Signaling Technology), mouse anti-activated β-catenin (1:50; Millipore), rabbit anti-IkBα (1:25; Abcam), rabbit anti-phospho-NF-kB p65 (Ser 311) (1:100; Santa Cruz Biotechnology), rabbit phospho-p44/42 MAPK (ERK1/2) (Thr202/Tyr204) (1:100; Cell Signaling Technology), rat anti-mouse Ly-6G and Ly-6C Gr1 (1:250; BD Pharmingen), rabbit anti-CD11b (1:3000; Abcam), rabbit anti-CD163 (1:500; Santa Cruz Biotechnology), rat anti-CD68 (1:200; Abcam), and rabbit anti-S100A4 (gift from Eugene Lukanidin). The negative controls omitted the primary antibody. Detection was achieved with the Liquid DAB + Substrate Chromogen System (Dako). All of the slides were counterstained with Gill's hematoxylin (Bio-Optica). For statistical analysis, both positive nuclei/cells and total cells were counted in three random fields per section under 40× magnification, and the percentages of positive cells in each field were calculated from the sections obtained from at least three different mice. Then the average of %positive nuclei/cells in each field per section was calculated and the statistical analysis was performed.

ELISA assays

Blood samples were collected from vehicle- and dipyridamole-treated mice after the mammary fat-pad implantation and allowed to clot. The sera were separated by centrifugation at 3,000×g for 30 min, and immediately frozen and stored at −80 °C until use. Interleukin-1α (IL-1α), interleukin-1β (IL-1β), granulocyte colony stimulating factor (G-CSF), granulocyte–macrophage colony stimulating factor (GM-CSF), monocyte chemotactic protein 1 (MCP-1), macrophage inflammatory protein 1a (MIP-1a), stem cell factor (SCF), and Rantes cytokines levels were analyzed in the sera collected, using the Mouse Inflammation ELISA Strip for Profiling 8 Cytokines (Signosis BioSignal Capture), according to the manufacturer protocol.

Statistical analysis

The statistical comparisons of the data from the in vitro and in vivo treatments were performed using Students' t test and ANOVA, respectively. Statistical significance was established at $p \leq 0.05$.

Fig. 1 In vitro effects of dipyridamole. **a** Representative cell proliferation assay (of two experiments performed with similar results) with 4T1-Luc and MDA-MB-231T cells treated with PBS-PEG (control) or dipyriramole (as indicated). Data are mean ± SE. *$p < 0.001$, **$p < 0.035$ (Students' t test). **b** Representative dynamic monitoring of cell proliferation (each with two experiments performed with similar results) of 4T1-Luc (*left panel*) and MDA-MB-231T (*right panel*) cells treated with DMSO (control) or 50 μM dipyridamole (as indicated). *Arrows*, time of vehicle/dipyridamole addition, to which cell index (CI) values were normalized. Data are mean ± SD. **c** Representative FACS analysis for cell-cycle phases (of two experiments performed with similar results) of 4T1-Luc and MDA-MB-231T cells treated for 24 h with PBS-PEG or dipyridamole (as indicated). Data are mean ± SE. *$p < 0.01$ (Students' t test). **d** Immunoblotting for cyclin D1 in 4T1-Luc and MDA-MB-231T cells treated for 24 h with PBS-PEG or dipyridamole (as indicated). β-actin used as control for equal loading. **e** p27 gene expression in 4T1-Luc and MDA-MB-231T cells treated for 24 h with PBS-PEG or dipyridamole (as indicated). Data are mean ± SEM. **f** Representative FACS analysis for apoptosis evaluation (of two experiments performed, with similar results) of 4T1-Luc and MDA-MB-231T cells treated for 24 h with PBS or dipyridamole (as indicated). Data are mean ± SE

Results

Dipyridamole impairs in vitro cell growth

To assess the dipyridamole ability to impair cell growth, in vitro cell proliferation assays were performed on triple-negative murine 4T1-Luc and human MDA-MB-231T breast-cancer cells. Dipyridamole decreased the proliferation of both the 4T1-Luc and the MDA-MB-231T cells, in dose- and time-dependent manners, as compared to the PBS-PEG–treated (control) cells (Fig. 1a). Dipyridamole significantly reduced the proliferation of both of these cell lines at almost all of the experimental points tested (Fig. 1a; 4T1-Luc, $p < 0.001$; MDA-MB-231T $p < 0.035$; Students' t test). The exception here was 24 h treatment of 4T1-Luc cells with 10 μM dipyridamole, as compared to these PBS-PEG–treated cells ($p = 0.2$, Students' t test).

Similar results were obtained in real-time proliferation assays using the xCelligence System. Dipyridamole-treated 4T1-Luc cells did not show any significant changes in their CI during the first hours after dipyridamole addition; this was followed by a significant reduced increase in CI, as compared to the vehicle (DMSO) control (Fig. 1b, left panel). With the MDA-MB-231T cells, dipyridamole caused a transient decrease in CI during the first hours after its addition, which was then followed by a significant reduced increase in CI of these dipyridamole treated cells, as compared to the vehicle (DMSO)-treated cells (Fig. 1b, right panel).

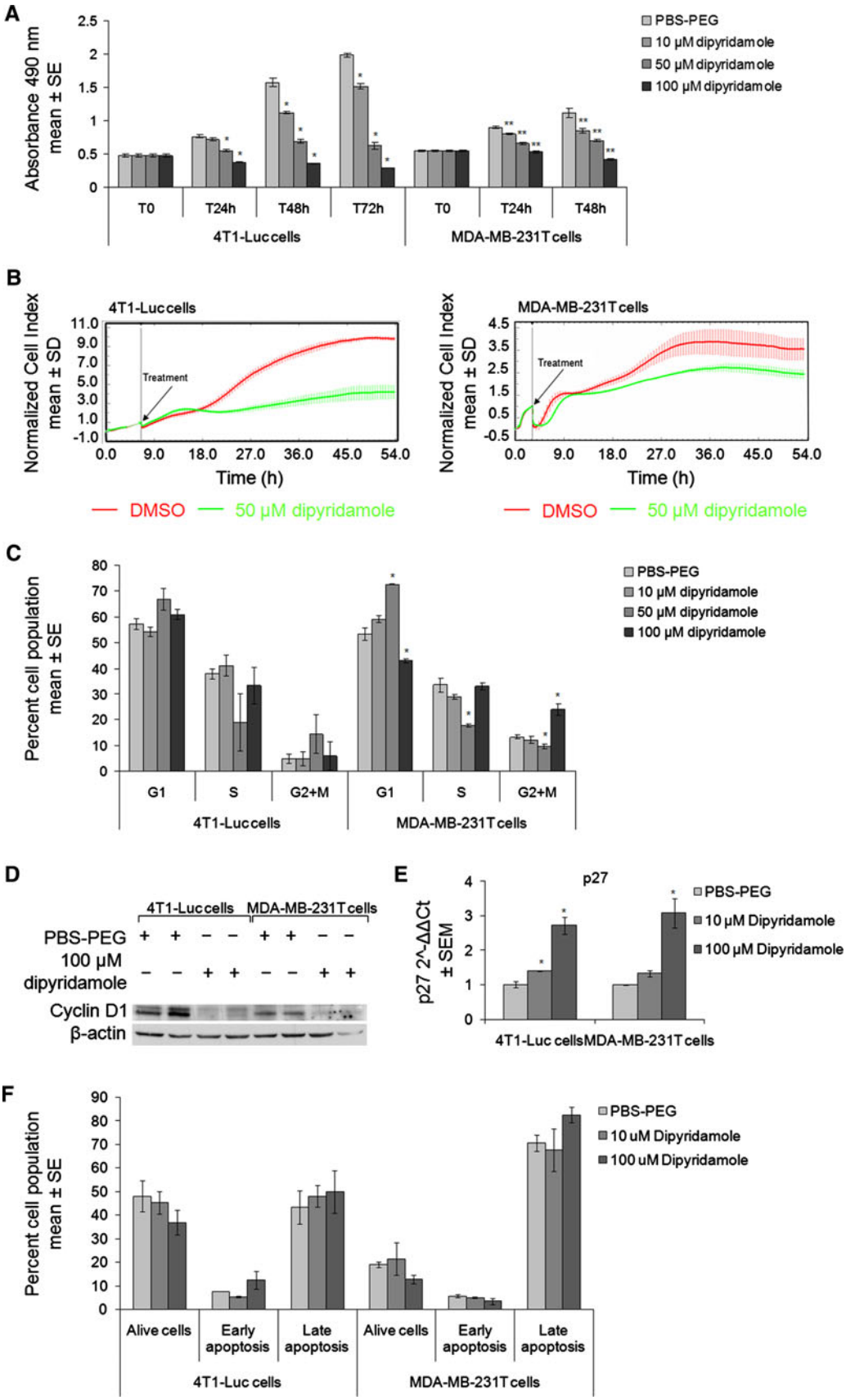

To unravel the molecular mechanisms involved in this dipyridamole-induced reduction of cell proliferation, we analyzed cell-cycle perturbation by dipyridamole. Significant effects were seen on the cell cycle at 50 μM dipyridamole only for the MDA-MB-231T cells, which resulted in a 19.3 % increase in the G_1-phase cell population, as compared to the PBS-PEG–treated cells (Fig. 1c; $p = 0.0013$, Students' t test). To further address dipyridamole-induced impairment of cell proliferation, the levels of cyclin D1 protein (which promotes progression through the G_1-S phase of the cell cycle) and p27 mRNA (a cyclin-dependent kinase inhibitor that blocks the cell cycle in the G_0/G_1 phase) were measured by Western blotting and qRT-PCR respectively. Dipyridamole determined a significant depletion of cyclin D1 protein both in 4T1-Luc and MDA-MB-231T cells as compared to the PBS-PEG–treated (control) cells (Fig. 1d). Similarly, a significant increased expression of p27 mRNA was observed in both dipyridamole-treated 4T1-Luc and MDA-MB-231T cells as compared to the PBS-PEG–treated (control) cells (Fig. 1e; 4T1-Luc, 10 μM dipyridamole $p = 0.044$, 100 μM dipyridamole $p = 0.022$; MDA-MB-231T, 100 μM dipyridamole $p = 0.039$; Students' t test).

We also analyzed the perturbation in apoptosis caused by this dipyridamole treatment, using an Annexin V assay. As shown in Fig. 1f, although the dipyridamole determined a decrease in percent population of alive cells and a corresponding increase in percent population of apoptotic cells as compared to PBS-PEG–treated cells, these changes did not reach statistical significance. Then a caspase-3 activity assay with the 4T1-Luc cells showed a small, but significant, effect on apoptosis at 50 and 100 μM dipyridamole (Fig. S1; $p = 0.03$ for both, Students' t test). These data thus support the concept that the impairment of cell proliferation observed in the 4T1-Luc and MDA-MB-231T cells is related to an arrest in the G_1 phase of the cell cycle, thus further strengthening the results already presented by Goda and collaborators [15].

In summary, dipyridamole inhibited cell proliferation in both these two triple-negative breast-cancer cell lines.

Dipyridamole impairs in vitro cell motility

To determine dipyridamole effects on cell migration, in vitro cell motility assays were performed with these 4T1-Luc and MDA-MB-231T breast-cancer cells. Here, 50 and 100 μM dipyridamole significantly impaired 4T1-Luc cell migration in a dose-dependent manner (Fig. 2a; $p = 0.039$, 0.018, respectively, Students' t test). Similarly, 100 μM dipyridamole treatment almost completely blocked MDA-MB-231T cell motility (Fig. 2b; $p < 0.0001$, Students' t test).

In summary here, dipyridamole inhibited cell motility in both these two breast-cancer cell lines.

Dipyridamole impairs in vivo primary tumor growth

Dipyridamole was further investigated in an in vivo 4T1-Luc breast-cancer xenograft mouse model. To determine the effects of dipyridamole on primary tumor growth, the 4T1-Luc cells were orthotopically implanted into the mammary fat pads of Balb/c syngeneic mice. In the first set of experiments, 5×10^4 4T1-Luc cells were implanted. Vehicle (PBS-PEG control) or dipyridamole (15 or 30 mg/kg/day for 5 days/week) were administered intraperitoneally beginning on day 7 post-implantation. Both of these dipyridamole treatments showed significant reductions in the primary tumor volume compared to the PBS-PEG control mice (Fig. S2). At the 15 mg/kg/day dose, dipyridamole inhibited the mean tumor size on day 21 post-implantation by 67.5 %, as compared to the control (Fig. S2A; $p = 0.0433$, ANOVA). At the higher, 30 mg/kg/day, dipyridamole dose, there was essentially no tumor growth in the dipyridamole-treated animals (Fig. S2B; $p = 0.0182$, ANOVA).

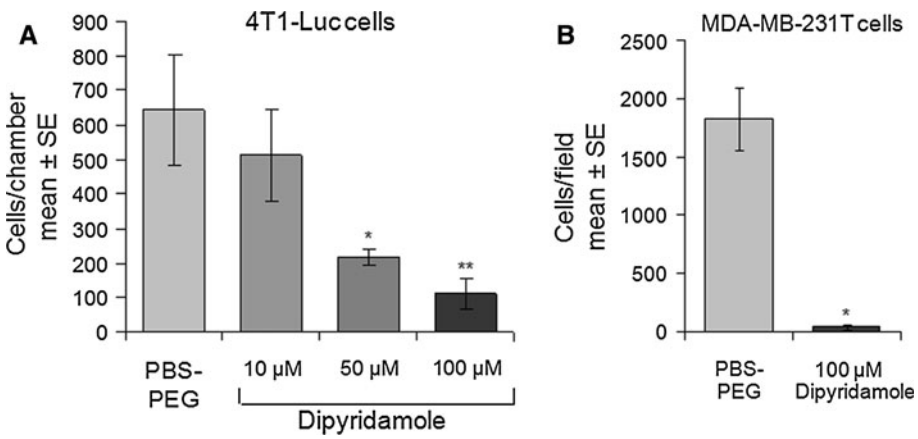

Fig. 2 Dipyridamole impairs cell motility. Representative motility assays (each with two experiments performed with similar results) in 4T1-Luc (**a**) and MDA-MB-231T (**b**) cells treated for 4 h with PBS-PEG or dypiridamole (as indicated). Data are mean ± SE. **a** $*p = 0.039$, $**p = 0.018$. **b** $*p < 0.0001$ (Students' t test)

To confirm these data, the number of cells implanted into the mammary fat pad of these Balb/c syngeneic mice was increased (by fivefold, to 2.5×10^5 4T1-Luc cells) and the beginning of the vehicle and dipyridamole treatments was delayed to day 14 post-implantation. At this stage, the mean tumor size according to the BLI measurements was at least one order of magnitude greater than the primary tumors treated in the initial experiments. At the same time, the intraperitoneal dipyridamole treatment was increased to 60 mg/kg/day (5 days/week). Figure 3a (on the left) shows representative images of these PBS-PEG control and dipyridamole-treated mice following the 4T1-Luc cell implantation (day 0) and at 42 days post-implantation. Overall, the mice treated with dipyridamole showed a significant 76.7 % reduction in tumor volume on day 42 post-implantation, as compared to the controls (Fig. 3a on the right; $p = 0.0429$, ANOVA).

To further demonstrate the dipyridamole impairment of primary tumor growth, the levels of Ki67, a marker of tumor-cell proliferation, were assessed by IHC on sections from the tumors of vehicle- and dipyridamole-treated mice. Representative images of Ki67 staining are shown in Fig. 3b, while the quantification shown in Fig. 3c illustrates that overall, the percentage of Ki67-positive tumor cells nuclei was significantly reduced by 19.7 % in tumors from those dipyridamole treated mice, as compared to those from the control mice ($p = 0.0032$, ANOVA). The cleaved caspase-3 levels, a marker of apoptosis, were also determined by IHC on tumor sections from these vehicle- and dipyridamole-treated mice. However, no significant differences were seen between the percentages of cleaved-caspase-3-positive tumor cells of tumors from these vehicle- and dipyridamole-treated mice (Fig. S3A; $p = 0.0962$, ANOVA).

In summary, intraperitoneally delivered dipyridamole inhibited in vivo 4T1-Luc primary tumor growth over a range of inocula.

Dipyridamole impairs in vivo metastases

To determine the effects of dipyridamole on metastasis foci formation and growth, experimental metastasis assays were conducted using both the 4T1-Luc and MDA-MB-231T cells. The 4T1-Luc cells were injected into the arterial circulation via the left cardiac ventricle of Balb/c syngeneic mice. The vehicle (PBS-PEG control) and the dipyridamole (30 mg/kg/day for 5 days/week) were administered intraperitoneally beginning on day 7 post-injection, at which time a few metastatic foci were detected by BLI (data not shown). In Fig. 3d (on the left) the representative images of mice on the day of injection (day 0) and at week 3 post-injection (2 weeks of treatment) show widespread metastatic involvement in the control mice, and visibly fewer and smaller metastatic foci in the dipyridamole-treated mice. The overall BLI data analysis shows that the total flux per mouse was decreased by 50.3 % in the dipyridamole treated mice, as compared to the vehicle-treated mice (Fig. 3d on the right; $p = 0.0292$, ANOVA).

In the parallel MDA-MB-231T model, 1×10^6 MDA-MB-231T cells were injected into the tail vein of nude mice, and lung metastasis formation was analyzed. The vehicle (PBS-PEG control) and the dipyridamole (30 mg/kg/day for 6 days/week) were administered either intraperitoneally or by oral gavage, to also determine the clinical efficacy in a comparison of these delivery modes in vivo. Administration started on day 1 post-injection. Figure 3e (on the left) shows representative images of the mouse lungs from day 45 post-injection. The count of the surface pulmonary metastases showed that dipyridamole did not inhibit metastasis formation when it was administered by oral gavage, while intraperitoneal delivery of dipyridamole resulted in a significant overall 47.5 % reduction in these mean pulmonary metastases, as compared to the lungs of the control mice (Fig. 3e on the right; $p = 0.0122$, ANOVA).

The Ki67 and cleaved caspase-3 levels were also determined by IHC on sections of the lung metastases from these intraperitoneally vehicle- and dipyridamole-treated mice. There were no significant differences in the percentages of Ki67-positive tumor cells nuclei or cleaved-caspase-3-positive tumor cells between these lung metastases from the control and the dipyridamole-treated mice (Fig. S3B and C respectively; $p = 0.5355$, $p = 0.1888$ respectively, ANOVA).

In summary, intraperitoneal delivery of dipyridamole inhibited metastasis formation in two model systems of triple-negative breast cancer. In particular, the dipyridamole-induced inhibition of metastasis formation in this MDA-MB-231T breast-cancer mouse xenograft model suggests that dipyridamole can be considered as a metastasis-preventing agent, as it was administered a day after the tumor-cell injection, when the circulating tumor cells were not yet established in the lung. On the other hand, the therapeutic efficacy of dipyridamole in metastasis treatment is suggested by its efficacy to inhibit metastasis formation in this 4T1-Luc breast-cancer mouse xenograft model, in which the treatment was delayed to day 7 after tumor-cell injection, when a few metastatic foci could already be detected.

In all of these mouse experiments, there were neither behavioral changes nor weight loss due to potential drug toxicity in these dipyridamole-treated mice, as compared to the control mice. This is also illustrated by the weights of the athymic nude mice that were injected with MDA-MB-231T cells, as given in Figure S4, where there were no signs of drug toxicity.

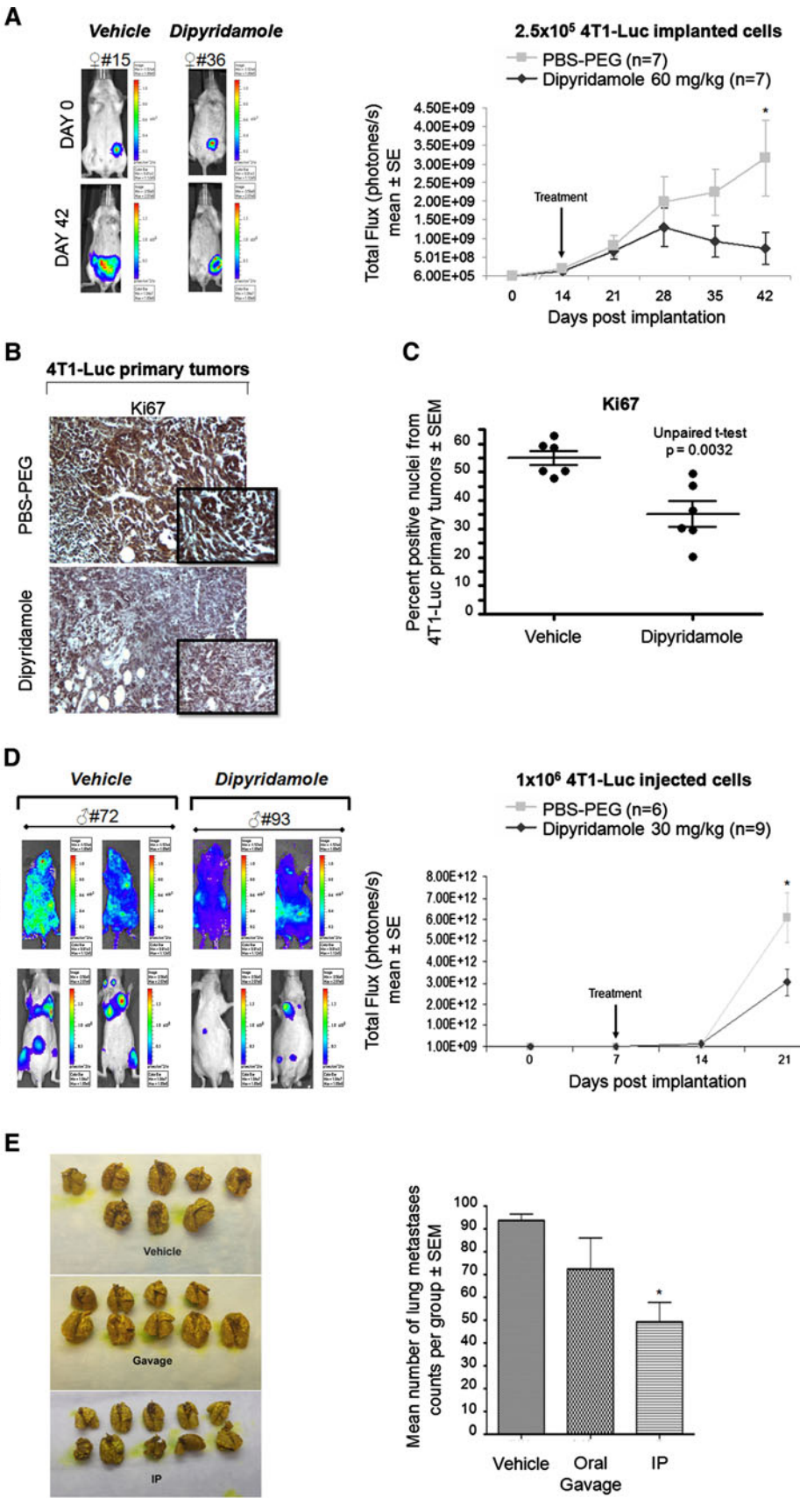

◀ **Fig. 3** Dipyridamole impairs primary tumor growth and metastasis in vivo. **a** On the *left*: representative bioluminescent images of mice implanted with 4T1-Luc cells in the mammary fat pad at day 0 and 42 days after intraperitoneally administered treatments with vehicle and 60 mg/kg/day dipyridamole (i.e. 4 weeks treatment). On the *right*: time-course of bioluminescent signals from 4T1-Luc tumor cells implanted into mouse mammary fat pad at day 0, followed by intraperitoneally administered treatments with vehicle and 60 mg/kg/day dipyridamole on day 14. Data are total flux mean ± SE. $*p = 0.0429$ (ANOVA). **b** Representative images of Ki67 IHC in sections of 4T1-Luc primary tumors from **a**. **c** Percentages of Ki67 positive tumor cells nuclei in sections of 4T1-Luc primary tumors from **a**. Data are mean ± SEM. $p = 0.0032$ (ANOVA). **d** On the *left*: representative bioluminescent images of mice intracardiacally injected with 4T1-Luc cells at day 0 and at week 3, after week 1 treatments with vehicle and 30 mg/kg/day dipyridamole intraperitoneally administered (i.e. 2 weeks treatment). Ventral and dorsal photographs were taken for each mouse. On the *right*: representative time-course of bioluminescent signals (of two experiments performed with similar results) from mice injected intracardiacally with 4T1-Luc tumor cells. Data are total flux mean ± SE. $*p = 0.0292$, ANOVA. **e** On the *left*: representative images of lungs from athymic nude mice injected with MDA-MB-231T cells via the tail vein and treated with vehicle or 30 mg/kg/day dipyridamole, delivery either by oral gavage or intraperitoneally (IP; as indicated). On the *right*: lung metastasis counts from *left panel*. Data are mean ± SEM. $*p = 0.0122$ (ANOVA)

Dipyridamole inhibits key signaling pathways

The strong cytostatic effects of dipyridamole suggested that it can affect key signaling pathways in tumors. To identify these signaling pathways that are affected by dipyridamole, we analyzed dipyridamole-induced perturbations of activation of the AKT, ERK1/2-MAPK and Wnt signaling pathways in these 4T1-Luc cells. The expression levels of AKT and Ser 473 phosphorylated AKT proteins (P-AKT) were determined by western blotting analyses (Fig. 4a). As shown in Fig. 4b, no change in P-AKT/AKT ratio was observed in 4T1-Luc cells after in vitro dipyridamole treatment, which overall thus indicates that dipyridamole does not alter the activation of this signaling pathway. To analyze the dipyridamole-induced perturbation of ERK1/2-MAPK signaling pathway, we assessed by western blotting the expression levels and the phosphorylation states of ERK1/2 proteins, the major effectors of this signaling pathway (Fig. 4a). Significant reductions of phospho-ERK1/ERK1 (P-ERK1/ERK1) and phospho-ERK2/ERK2 (P-ERK2/ERK2) ratios were observed in 4T1-Luc cells after in vitro 100 μM dipyridamole treatment as compared to PBS-PEG–treated cells, thus resulting in an impairment of ERK1/2-MAPK pathway activation (Fig. 4b; P-ERK1/ERK1 $p = 0.017$; P-ERK2/ERK2 $p = 0.047$; Students' t test). Similarly to address the effect of dipyridamole on Wnt signaling pathway, the protein levels of β-catenin (a major effector of the canonical Wnt pathway), of GSK-3β (which in turn phosphorylates β-catenin thus causing its degradation and consequently the inhibition of Wnt pathway), and Ser 9 phosphorylated GSK-3β (P-GSK-3β; the GSK-3β inactivated form) were determined by western blotting analyses in 4T1-Luc cells after in vitro dipyridamole treatment (Fig. 4a). As shown in Fig. 4b, dipyridamole decreased the P-GSK-3β/GSK-3β ratio, thus determining in an increased activation of GSK-3β kinase activity, then resulting in an impairment of Wnt signaling. According to this data, the activated β-catenin levels were found reduced (Fig. 4a), which thus indicated dipyridamole-induced attenuation of the Wnt signaling pathway.

To further confirm these results, we transiently transfected HEK293T cells with the TOP/FOP-FLASH system [30], which allows the detection of β-catenin transcriptional activation by measuring luciferase reporter activity. After transfection, these cells were treated with PBS-PEG (as control vehicle) and dipyridamole, and their luciferase activities were measured. As shown in Fig. 4c, in absence of the plasmid encoding β-catenin the HEK293T cells transfected with the empty vector (pGL3) and with each of the plasmids of the TOP/FOP-FLASH system showed a very low level of normalized firefly luciferase activity. In the presence of the plasmid encoding β-catenin an increased level of normalized firefly luciferase activity was observed in those cells transfected with the TOP-FLASH plasmid containing four Tcf consensus binding sites upstream of firefly luciferase cDNA. As expected, the normalized firefly luciferase activity did not increase in those cells transfected with FOP-FLASH plasmid with mutated Tcf binding sites or with pGL3 vector. The dipyridamole treatment of HEK293T cells cotransfected with the plasmid encoding β-catenin and with the TOP-FLASH plasmid determined a significantly reduced increase of the normalized firefly luciferase activity as compared to the control cells (Fig. 4c; $p = 0.006$, Students' t test).

We then investigated this dipyridamole-induced Wnt pathway attenuation in terms of the expression of the CD49f, cyclin D1, survivin and c-Myc proteins, which are all early targets of the Wnt pathway [31]. Here, dipyridamole significantly decreased the percentage of 4T1-Luc breast-cancer cells that expressed the membrane antigen CD49f (Fig. 4d; $p = 0.008$, Students' t test), and as previously showed in Fig. 1d, significantly decreased the expression of cyclin D1. In parallel, in the MDA-MB-231T cells, dipyridamole significantly decreased the expression levels of all proteins including cyclin D1 (Fig. 1d), survivin and c-Myc (Fig. 4e).

Previous reports have shown that dipyridamole attenuates the activation of the NF-kB signaling pathway [32, 33]. Therefore, we investigated whether this was also the case in the 4T1-Luc breast-cancer cells, by determination of the expression levels of IkBα, an inhibitor of the NF-kB signaling pathway. Here, 4 h of in vitro dipyridamole treatment of the 4T1-Luc cells at both 10 and 100 μM did not alter the IkBα

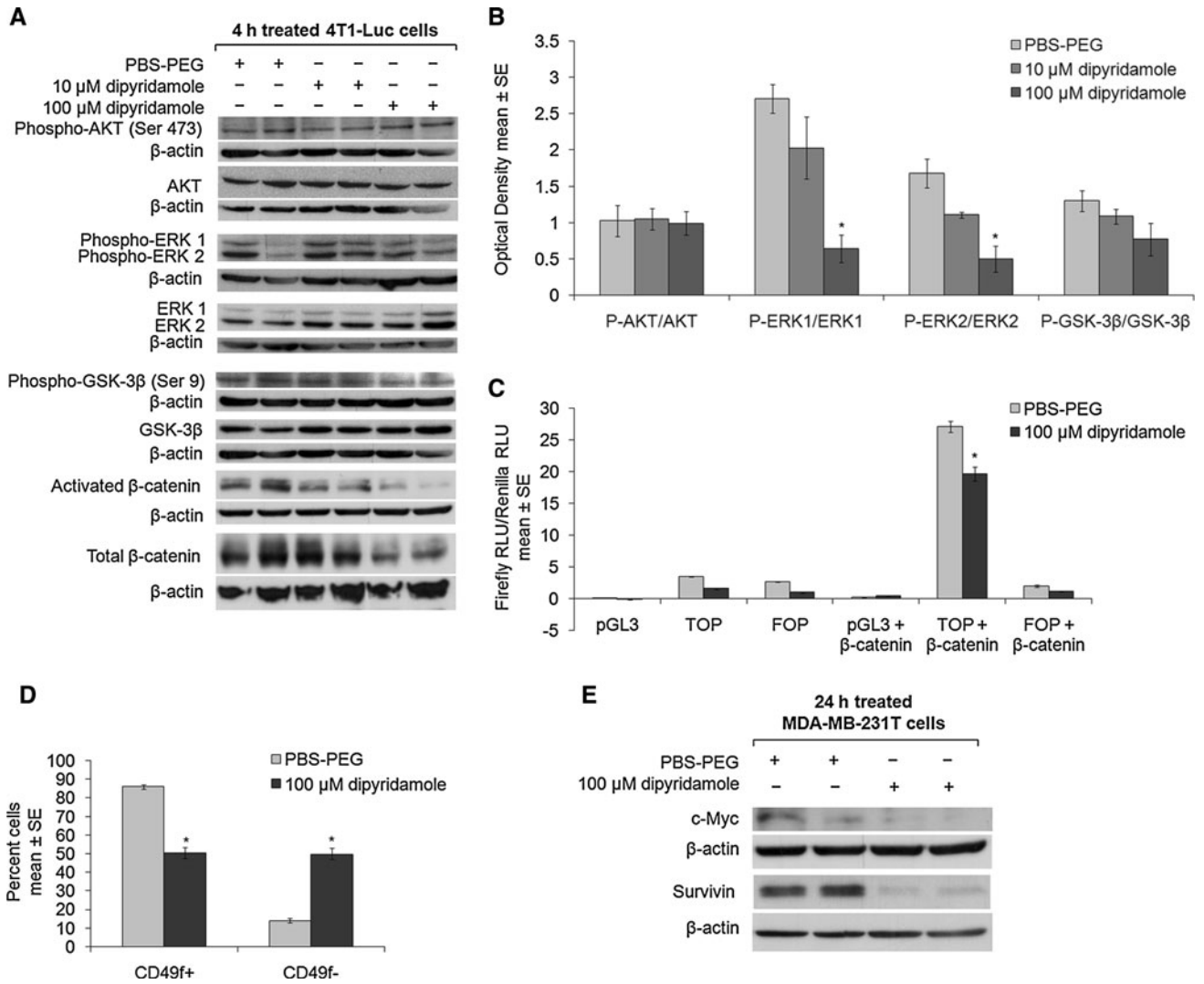

Fig. 4 Dipyridamole impairs Wnt and ERK1/2-MAPK signaling pathways in vitro. **a** Immunoblotting for phospho-AKT, AKT, phospho-ERK1/2, ERK1/2, phospho-GSK-3β, GSK-3β, total and activated β-catenin in 4T1-Luc cells treated for 4 h with PBS-PEG or dipyridamole (as indicated). β-actin used as control for equal loading. **b** The densitometer analyses for the proteins from **a**. Data are mean ± SE. *P-ERK1/ERK1 $p = 0.017$; P-ERK2/ERK2 $p = 0.047$ (Students' t test). **c** Representative luciferase activity in TOP/FOP FLASH system transfected HEK293T cells (of two experiments performed with similar results) after overnight treatment with PBS-PEG or dipyridamole (as indicated). Data are mean ± SE. *$p = 0.006$ (Students' t test). **d** Representative analysis for percentage positivity to CD49f, a known target of Wnt pathway, (of two experiments performed with similar results) of 4T1-Luc cells treated for 24 h with PBS-PEG or dipyridamole (as indicated). Data are mean ± SE. *$p = 0.008$ (Students' t test). **e** Immunoblotting for c-Myc and survivin in MDA-MB-231T cells treated for 24 h with PBS-PEG or dipyridamole (as indicated). β-actin used as control for equal loading

level (Fig. S5A). However, 24 h of treatment with 10 and 100 μM dipyridamole resulted in the up-regulation of IkBα (Fig. 5a), thus indicating dipyridamole-induced attenuation of the NF-kB signaling pathway. To further address this point, the expression levels of phosphorylated IkBα (P-IkBα), p65 and phosphorylated p65 (P-p65) proteins were determined by western blotting analyses (Fig. 5a). As shown in Fig. 5b, a reduction of both the P-IkBα/IkBα and P-p65/p65 ratios that reached the limit of significance was observed at 100 μM dipyridamole ($p = 0.06$, $p = 0.077$ respectively, Students' t test), which thus further suggests dipyridamole-induced attenuation of NF-kB signaling pathway. We then transiently cotransfected HEK293T cells with a plasmid encoding p65 and a plasmid containing the immunoglobulin promoter, which is responsive to p65, upstream of firefly luciferase cDNA (IgLuc vector). After transfection, these cells were treated with PBS-PEG (control-vehicle) and dipyridamole, and their luciferase activities were measured. As shown in Fig. 5c, in absence of the plasmid encoding p65 the HEK293T cells transfected with the empty vector (pGL3) and

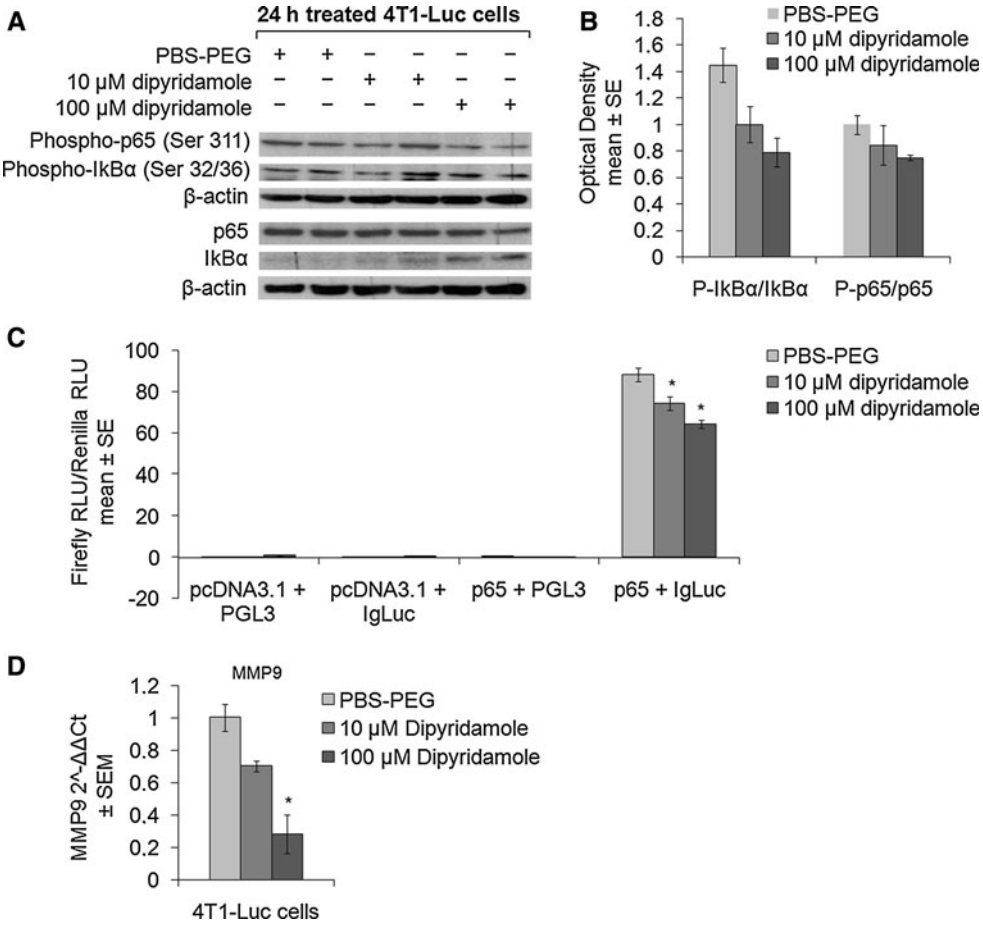

Fig. 5 Dipyridamole impairs NF-kB signaling pathway in vitro. **a** Immunoblotting for phospho-IkBα, IkBα, phospho-p65 and p65 in 4T1-Luc cells treated for 24 h with PBS-PEG or dipyridamole (as indicated). β-actin used as control for equal loading. **b** The densitometry analyses for the proteins from **a**. Data are mean ± SE. **c** Representative luciferase activity in p65 and IgLuc transfected HEK293T cells (of two experiments performed with similar results) after overnight treatment with PBS-PEG or dipyridamole (as indicated). Data are mean ± SE. *10 μM dipyridamole $p = 0.04$; 100 μM dipyridamole $p = 0.003$ (Students' t test). **d** Expression of MMP9 gene, a known target of NF-kB pathway, in 4T1-Luc cells treated for 24 h with PBS-PEG or dipyridamole (as indicated). Data are mean ± SEM. *$p = 0.039$ (Students' t test)

with IgLuc plasmid showed a low level of normalized firefly luciferase activity. In the presence of the plasmid encoding p65 an increased level of normalized firefly luciferase activity was observed in only those cells transfected with the IgLuc plasmid. As expected, the normalized firefly luciferase activity did not increase in those cells transfected with pGL3 vector, thus further confirming the specificity of responsiveness of immunoglobulin promoter within our in vitro assay. At this time, we found the dipyridamole treatment of HEK293T cells cotransfected with the plasmid encoding p65 and with Ig-Luc plasmid induced less of an increase in the normalized firefly luciferase activity as compared to the control transfected cells (Fig. 5c; 10 μM dipyridamole $p = 0.04$; 100 μM dipyridamole $p = 0.003$; Students' t test).

We then investigated this NF-kB pathway attenuation in terms of the expression of its main targets. We already showed the down-regulation of cyclin D1 (Fig. 1d), c-Myc and survivin (Fig. 4e), which are known to be early targets of both Wnt and NF-kB signaling pathways [34, 35]. To further validate this, we analyzed the expression of the MMP9 mRNA, another target of NF-kB [34], in 4T1-Luc cellular model. Here we found that 100 μM dipyridamole significantly decreased the MMP9 gene expression (Fig. 5d; $p = 0.039$, Students' t test).

In conclusion to exclude any unspecific target regulation, we verified the expression of phosphoglucokinase gene (PGK), which is known to be not a target of all those above mentioned signaling pathways (ERK1/2-MAPK, Wnt and NF-kB). PGK mRNA expression was analyzed by qRT-PCR. As shown in Figure S5B, dipyridamole did not alter the PGK gene expression. Although it is not still possible to specifically define at this time how mechanistically dipyridamole targets ERK1/2-MAPK, NF-kB and Wnt signaling pathways, the results here presented are showing no effect on AKT signaling pathway and on PGK gene expression, thus demonstrating some level of specificity of dipyridamole on those above mentioned pathways. Future studies will need to address how dipyridamole infer mechanistically those pathways.

We also investigated the in vivo ability of dipyridamole to impair the Wnt, ERK1/2-MAPK and NF-kB signaling pathways. Here, the percentages of tumor cells nuclei positive for activated β-catenin, phospho-p65 and phospho-ERK1/2 and the percentages of tumor cells positive for IkBα were also evaluated on tumor sections by IHC.

Representative images of activated β-catenin staining are shown in Fig. 6a. In the 4T1-Luc mammary fat-pad mouse xenograft model, the percentage of activated β-catenin-positive tumor cells nuclei was significantly reduced by 38.6 % in tumors from the dipyridamole-treated mice, as compared to those from the vehicle-treated mice (Fig. 6b; $p < 0.0001$, ANOVA). In the MDA-MB-231T cell in vivo experimental metastasis model, the percentage of activated β-catenin–positive tumor cells nuclei in lung metastases from mice treated intraperitoneally with dipyridamole was significantly reduced by 16.4 %, as compared to tumors from the control mice (Fig. 6c; $p = 0.0055$, ANOVA). However, there were no significant differences in the percentages of activated-β-catenin–positive tumor cells nuclei in the lung metastases following the oral gavage dipyridamole treatment in these mice, as compared to the control mice (Fig. 6c; $p = 0.8619$, ANOVA). In parallel, the expression levels of the cyclin D1 and c-Myc proteins were also reduced in these 4T1-Luc primary tumors from the dipyridamole-treated mice, as compared those from the control mice (Fig. S6).

Additionally we evaluated in vivo the phospho-ERK1/2 inhibition as already encountered in vitro. Representative images of phospho-ERK1/2 staining are shown in Fig. 6a. In the 4T1-Luc mammary fat-pad mouse xenograft model, the percentage of phospho-ERK1/2–positive tumor cells nuclei was significantly reduced by 6.4 % in tumors from the dipyridamole-treated mice, as compared to those from the vehicle-treated mice (Fig. 6d; $p = 0.0187$, ANOVA). In the MDA-MB-231T cell in vivo experimental metastasis model, the percentage of phospho-ERK1/2–positive tumor cells nuclei in lung metastases from these mice treated intraperitoneally with dipyridamole was significantly reduced by 25.05 %, as compared to tumors from the control mice (Fig. 6e; $p = 0.0129$, ANOVA). Similarly to the results obtained for the evaluation of activated β-catenin, there were no significant differences in the percentages of phospho-ERK1/2–positive tumor cells nuclei in the lung metastases following the oral gavage dipyridamole treatment in these mice, as compared to the control mice (Fig. 6e; $p = 0.135$, ANOVA).

Then we investigated in vivo the NF-kB pathway by measuring the number of IkBα– positive tumor cells in those treated animals. For IkBα (whose representative images are shown in Fig. 6a), in both the 4T1-Luc mammary fat-pad xenograft model and the MDA-MB-231T experimental metastasis model, intraperitoneally administered dipyridamole doubled the percentages of IkBα-positive tumor cells (Fig. 6f; $p = 0.0487$; Fig. 6g; $p = 0.0019$, respectively, ANOVA). Also, similar to that seen for activated β-catenin and phospho-ERK1/2, there were no significant differences in the percentages of IkBα-positive tumor cells in the lung metastases from the mice treated with oral gavage of dipyridamole, as compared to tumors from the control mice (Fig. 6g; $p = 0.0893$, ANOVA). According to the results for IkBα, in the 4T1-Luc mammary fat-pad mouse xenograft model, the percentage of phospho-p65–positive tumor cells nuclei (whose representative images are shown in Fig. 7a) was significantly reduced by 67.82 % in tumors from the dipyridamole-treated mice, as compared to those from the vehicle-treated mice (Fig. 7b; $p < 0.0001$, ANOVA). In the MDA-MB-231T cell in vivo experimental metastasis model, the percentage of phospho-p65–positive tumor cells nuclei in lung metastases from these mice treated both by oral gavage and intraperitoneally with dipyridamole was significantly reduced by 17.67 and 24.88 % respectively, as compared to tumors from the control mice (Fig. 7c; oral gavage administration $p = 0.0002$; intraperitoneal administration $p < 0.0001$; ANOVA). In this case, although both dipyridamole treatments resulted in a significant decrease of percentage of phospho-p65–positive tumor cells nuclei as compared to control tumors, the intraperitoneal administration of the drug was more effective than the oral gavage delivery. In fact the comparison between these two treatment groups showed the intraperitoneally delivered dipyridamole determined a significant reduced percentage of phospho-p65–positive tumor cells nuclei (7.21 %) as compared to tumors from mice administrated by oral gavage dipyridamole (Fig. 7c; $p = 0.0048$, ANOVA).

In summary, dipyridamole-induced inhibition of the Wnt, ERK1/2-MAPK and NF-kB signaling pathways was seen both in in vitro studies and in in vivo primary tumorigenesis and metastasis assays.

Fig. 6 Dipyridamole impairs signaling pathways in vivo. **a** Representative images of activated β-catenin, phospho-ERK1/2 and IkBα IHC in sections of 4T1-Luc primary tumors and MDA-MB-231T lung metastases from mice treated with intraperitoneally administered PBS-PEG or dipyridamole (as indicated). **b** Percentages of activated β-catenin positive tumor cells nuclei in sections of 4T1-Luc primary tumors from mice treated with intraperitoneally administered vehicle or dipyridamole (as indicated). Data are mean ± SEM. $p < 0.0001$ (ANOVA). **c** Percentages of activated β-catenin positive tumor cells nuclei in sections of lung metastases from athymic nude mice injected with MDA-MB-231T cells and treated with vehicle or dipyridamole (intraperitoneal or oral gavage administration). Data are mean ± SEM. Intraperitoneal administration $p = 0.0055$ (ANOVA). **d** Percentages of phospho-ERK1/2 positive tumor cells nuclei in sections of 4T1-Luc primary tumors as for **b**. Data are mean ± SEM. $p = 0.0187$ (ANOVA). **e** Percentages of phospho-ERK1/2 positive tumor cells nuclei in sections of lung metastases as for **c**. Data are mean ± SEM. Intraperitoneal administration $p = 0.0129$ (ANOVA). **f** Percentages of IkBα positive cells in sections of 4T1-Luc primary tumors as for **b**. Data are mean ± SEM. $p = 0.0487$ (ANOVA). **g** Percentages of IkBα positive cells in sections of lung metastases as for **c**. Data are mean ± SEM. Intraperitoneal administration $p = 0.0019$ (ANOVA)

Dipyridamole impairs the tumor microenvironment

The NF-kB pathway is critical for both the tumor cells and the inflammatory cells in the tumor microenvironment [36].

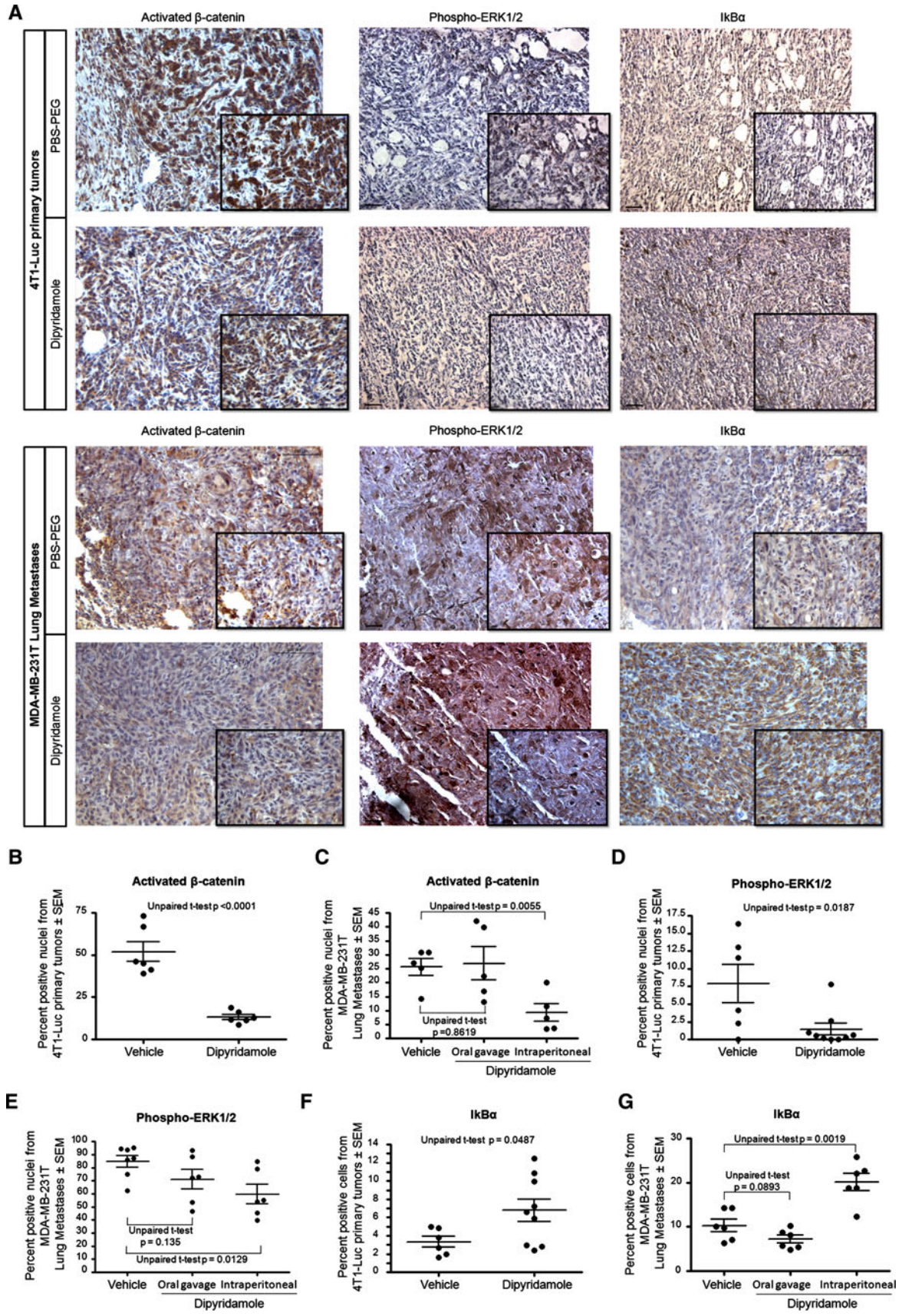

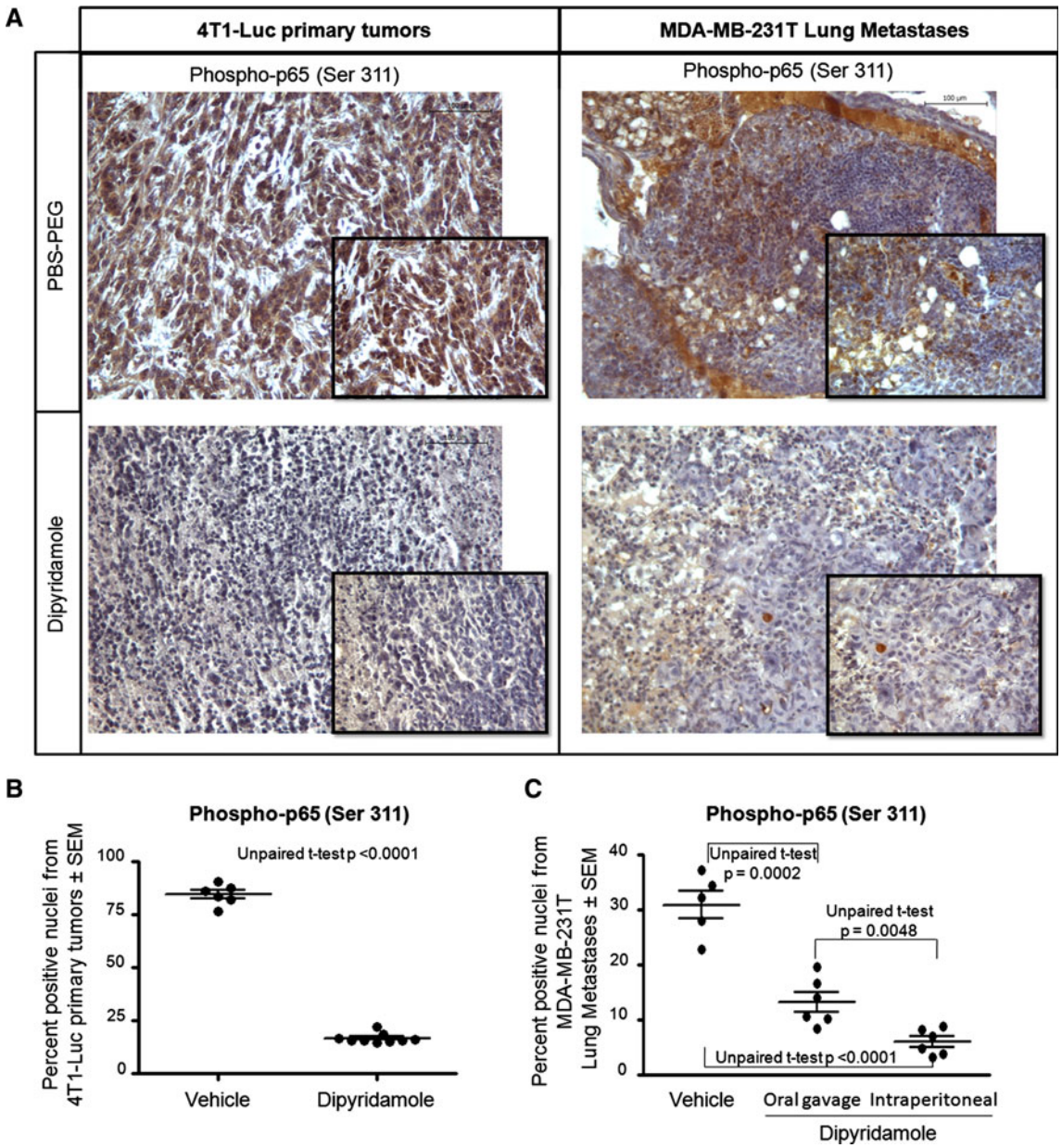

Fig. 7 Dipyridamole decreases the nuclear expression of phospho-p65 in vivo. **a** Representative images of phospho-p65 IHC in sections of 4T1-Luc primary tumors and MDA-MB-231T lung metastases from mice treated with intraperitoneally administered PBS-PEG or dipyridamole (as indicated). **b** Percentages of phospho-p65 positive tumor cells nuclei in sections of 4T1-Luc primary tumors from mice treated with intraperitoneally administered vehicle or dipyridamole (as indicated). Data are mean ± SEM. $p < 0.0001$ (ANOVA). **c** Percentages of phospho-p65 positive tumor cells nuclei in sections of lung metastases from athymic nude mice injected with MDA-MB-231T cells and treated with vehicle or dipyridamole (intraperitoneal or oral gavage administration). Data are mean ± SEM. Intraperitoneal administration $p < 0.0001$ (ANOVA)

To determine the effects of dipyridamole treatment on immune-cell infiltration into the tumor microenvironment, IHC analyses of tumor-associated macrophages (TAMs) and myeloid-derived suppressor cells (MDSCs) were conducted on sections of primary tumors from the breast cancer xenograft mice implanted with 4T1-Luc cells into the mammary fat-pad that had been intraperitoneally treated with vehicle (PBS-PEG) or 60 mg/kg/day (5 days per week) dipyridamole. Representative images of this staining are shown in Fig. 8a. For both the MDSCs ($CD11b^+$ and $Gr1^+$ cells) (Fig. 8b, c) and TAMs ($CD163^+$ and $CD68^+$ cells) (Fig. 8d, e), infiltration into the tumor microenvironment was significantly decreased by dipyridamole treatment, as compared to vehicle treatment (Gr1, $p = 0.0042$; CD163, $p = 0.0007$; other markers, $p < 0.0001$, ANOVA).

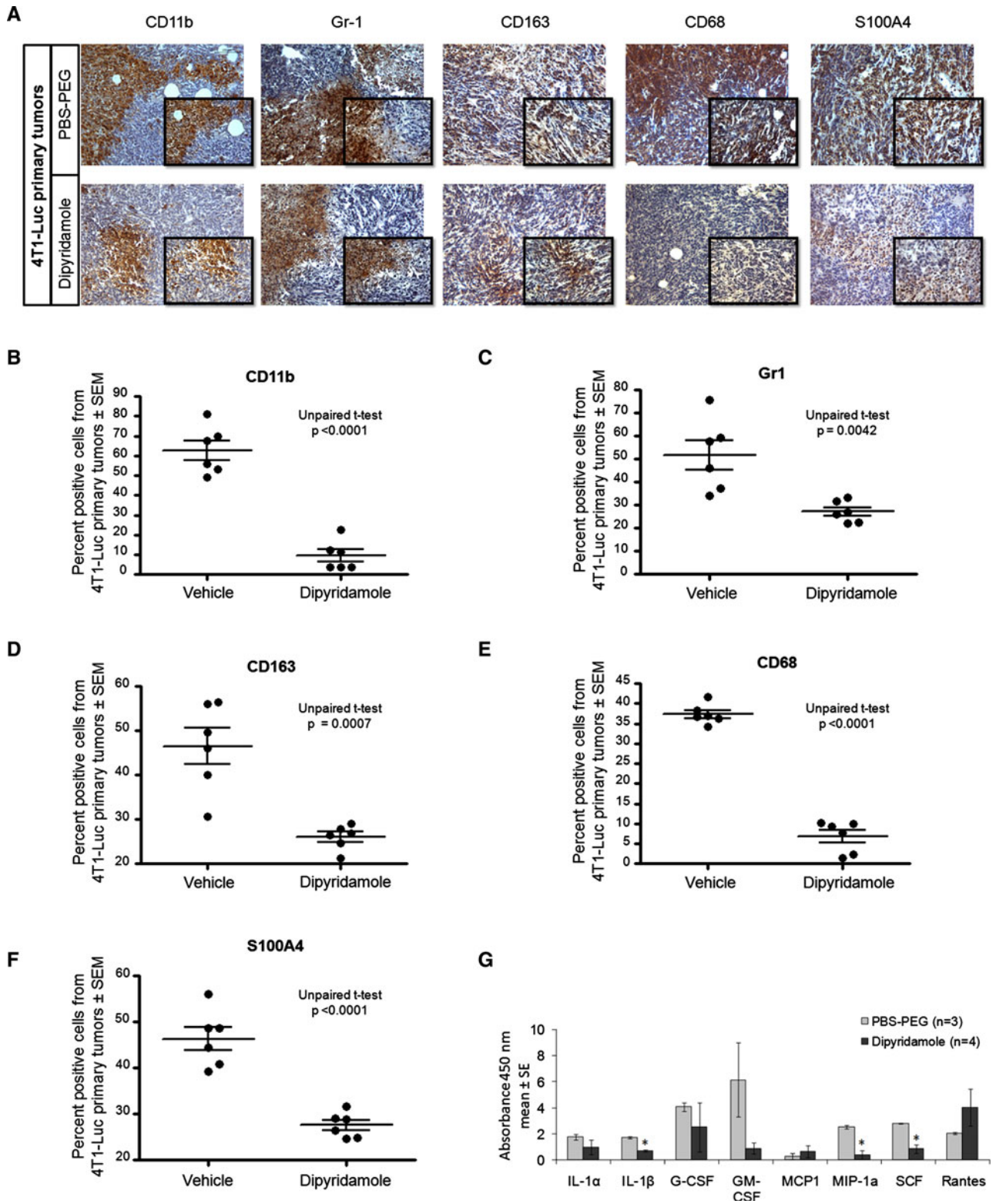

Fig. 8 Dipyridamole impairs tumor microenvironment and serum inflammatory cytokine levels. **a** Representative images of CD11b, Gr1, CD163, CD68 and S100A4 IHC in sections of 4T1-Luc primary tumors from mice treated with intraperitoneally administered PBS-PEG or dipyridamole (as indicated). **b**–**f** Percentage of cells positive to CD11b **b**, Gr1 **c**, CD163 **d**, CD68 **e** and S100A4 **f** in sections of 4T1-Luc primary tumors as for **a**. Data are mean ± SEM. **b**, **e**, **f** $p < 0.0001$; **c** $p = 0.0042$; **d** $p = 0.0007$ (ANOVA). **g** Absorbances for serum cytokine levels from 4T1-Luc cell implanted mice treated with PBS-PEG or dipyridamole (as indicated). Data are mean ± SE. * IL-1β, $p = 0.01$; MIP-1a, $p = 0.03$; SCF, $p = 0.03$ (Students' t test)

In the tumor microenvironment, we additionally analyzed the S100A4 protein, a calcium-binding protein of the S100 protein family, which has an important role in promoting cancer metastasis and invasion [37]. As S100A4 is a target of the Wnt pathway [38] and an activator of the NF-kB pathway [39], we investigated S100A4 protein levels using IHC on sections of the primary tumors from the breast-cancer xenograft mice that were implanted with 4T1-Luc cells into the mammary fat pad and intraperitoneally treated with vehicle or 60 mg/kg/day (5 days per week) dipyridamole. Representative images of this staining are shown in Fig. 8a. Here, dipyridamole significantly decreased the percentage of S100A4-positive cells by 18.7 % (Fig. 8f; $p < 0.0001$, ANOVA).

In addition, the NF-kB signaling pathway regulates cytokines production in inflammatory cells [40]. Based on these data, we further asked whether this intraperitoneal dipyridamole treatment can influence the serum levels of the cytokines in this breast-cancer xenograft mouse model. Here, the 60 mg/kg/day (5 days per week) dipyridamole treatment of the xenograft mice implanted with 4T1-Luc cells into the mammary fat pad significantly reduced the serum levels of IL-1β, MIP-1a and SCF, as compared to the vehicle treatment (Fig. 8g; $p = 0.01$, $p = 0.03$, $p = 0.03$, respectively, Students' t test), with similar trends seen for other cytokines tested (Fig. 8g; IL-1α, G-CSF, GM-CSF). Therefore, dipyridamole has in vivo effects on the NF-kB pathway in both tumor cells and the tumor microenvironment, which results in negative regulation of the inflammatory response.

Discussion

In current therapeutic practice, dipyridamole is rarely used as a single agent. However, an extended-released form of dipyridamole (Persantin Retard 200 mg) in combination with aspirin (25 mg) has been designed to take advantage of the additive antiplatelet effects of both of these agents, and this combination is used for secondary stroke prevention [19]. Based on the in vitro evidence that dipyridamole can modulate the cytotoxicity of a variety of antitumor agents [6–12], phase I and phase II clinical trials of the combination of dipyridamole and cytotoxic agents were performed in patients with advanced refractory malignancy [22–24, 41, 42]. Unfortunately, in these clinical trials, there were disappointing results in terms of the shrinkage of the established refractory metastases .

In the present study, we have demonstrated cytostatic and motility inhibitory effects of single-agent dipyridamole in vitro, with the concomitant reduction of primary tumor growth and metastasis formation in vivo. These conflicting results appear to be attributed to the mode of drug delivery. Indeed, previous studies showed that, depending upon the mode of delivery, a broad range of free dipyridamole concentrations is achieved with the intraperitoneal infusion more efficient than oral administration or intravenous infusion [43–45]. This is in keeping with our data, as we show that administration of dipyridamole by oral gavage is ineffective in reducing metastasis formation, while intraperitoneal delivery of dipyridamole results in significant reductions in metastasis formation in both of the breast-cancer xenograft mouse models used here. Based on these data, it is probable that the limited success of dipyridamole in the previous clinical trials can be ascribed to its delivery mode (oral administration or intravenous infusion) [22–24, 41, 42]. Based on our data, we propose that dipyridamole can be used in the clinic both as a therapeutic agent for the treatment of triple-negative breast-cancer primary tumors and as a preventive and therapeutic agent for the treatment of triple-negative breast-cancer metastasis. Translation of these data into the clinic awaits further pharmacokinetic studies.

Another limitation to the clinical application of dipyridamole has been its extensive binding to the serum protein α_1 acid glycoprotein (AGP) [46], an acute-phase protein that is elevated in the plasma of cancer patients. The avid binding of dipyridamole to AGP decreases the free plasma concentrations of dipyridamole to levels that are insufficient for its therapeutic effects [47]. Recently, a liposome-based intravenous delivery strategy of dipyridamole in combination with perifosine was used for inhibition of metastasis in a breast-cancer xenograft model [25, 26]. This approach thus has the potential to be applied to clinical trials in humans, to improve the distribution and delivery of dipyridamole, and to prevent the binding of dipyridamole to AGP. Additional studies will be required to address the dipyridamole delivery mode (intraperitoneal or intravenous delivery by liposomes) and to refine a proposed dose and schedule for dipyridamole treatment that can be included in a clinical trial.

Several molecular mechanisms might be responsible for the in vivo therapeutic efficacy of dipyridamole. In Fig. 9, we summarize the signaling pathways and the biological processes affected by dipyridamole here investigated at this time. A few insights on molecular mechanisms by which dipyridamole inhibits cell proliferation were provided by Goda and collaborators [15], who described a novel mechanism of dipyridamole induced G1 arrest in human osteosarcoma and prostate carcinoma cells [15]. In this study we further confirm the dipyridamole induces in vitro G1 cell cycle arrest in breast cancer cells and provide evidence that dipyridamole impairs in vivo the breast cancer tumor growth in 4T1-Luc breast cancer xenograft models. In an effort to further unravel the molecular mechanism of dipyridamole-induced proliferation inhibition we examined

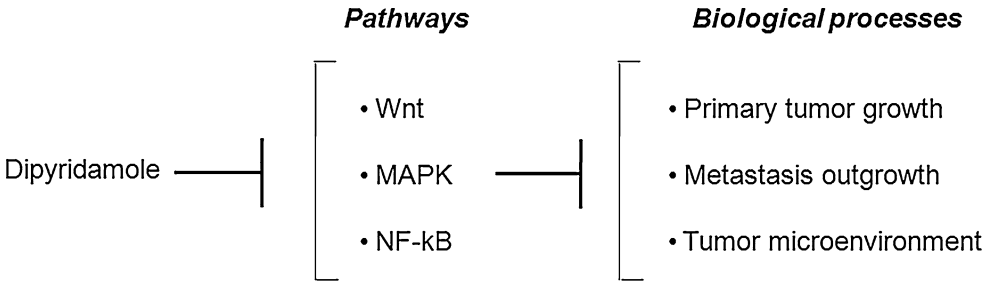

Fig. 9 Model of dipyridamole actions. The model shows the signaling pathways and the biological processes affected by dipyridamole

the signaling pathways perturbation by dipyridamole. Previous data have established that dipyridamole can attenuate the NF-kB signaling pathway [32]. In the present study, we also provide evidence that both in vitro and in vivo, dipyridamole can attenuate the Wnt signaling pathway, through reduced β-catenin activation, ERK1/2-MAPK signaling pathway, through the reduced phosphorylation of ERK1/2, and the NF-kB signaling pathway, through increased IkBα expression levels, decreased phosphorylation of p65 and reduced inflammatory cytokines systemic production (including IL-1β, which is activated by NF-kB with an activation feedback loop). As all of these signaling pathways promote cell proliferation, their dipyridamole-induced attenuation might represent a molecular mechanism by which dipyridamole can reduce tumor growth.

Literature data provides evidence of ERK1/2-MAPK signaling in cell migration [48]. Activated ERK regulates membrane protrusions and focal adhesion turnover via phosphorylating the myosin light chain kinase (MLCK) and promotes focal adhesion disassembly via phosphorylating and activating calpain protein signal. Moreover the phosphorylation of FAK and paxillin by ERK may regulate focal adhesion dynamics, probably by influencing the paxillin-FAK interaction [48]. Therefore, the ability of dipyridamole to impair cell motility and metastasis process might be due to its inhibitory effects on the ERK1/2-MAPK signaling pathway.

Signaling systems feature extensive crosstalk, and thereby form a complex network of interactions. Several previous studies have also shown that Wnt and NF-kB pathways are linked to each other by a positive-feedback loop. Kaler et al. described IL-1β as an activator of the Wnt signaling pathway that acts in a NF-kB-dependent manner [49]. This suggests that in vivo, the dipyridamole-induced Wnt pathway attenuation can be further enhanced by decreased IL-1β expression due to the impairment of the NF-kB signaling pathway. On the other hand, attenuation of the Wnt signaling pathway can lead to decreased expression of S100A4 [38], an important player in tumor progression and metastasis, and an activator of the NF-kB signaling pathway [39], thus further attenuating this latter pathway. A crosstalk with a positive-feedback loop between the Wnt and ERK pathways has been identified in tumor cells [50]. The activated ERK induces GSK-3β inhibition, which stops β-catenin degradation leading to its accumulation and translocation into the nucleus where β-catenin forms a complex with TCF. The β-catenin/TCF complex enhances the expression or activation of the unknown crosstalk molecules which then activates ERK via stimulation of Raf-1 and MEK, thus further perpetuating the activation loop [50]. Interestingly, a crosstalk between ERK-MAPK signaling and NF-kB pathway was already identified, in which ERK targets IKKα that in turn phosphorylates IkBα, thus activating NF-kB signaling pathway [51]. Although the data here presented show that dipyridamole inhibits Wnt, ERK1/2-MAPK and NF-kB pathways, at this time it is not possible to determine whether dipyridamole directly affects at the same time and all of those pathways. In fact the extensive crosstalk between these pathways opens the possibility that dipyridamole might target only one or two of these pathways with consequences on the other(s). The positive-feedback loop between Wnt and ERK pathways strength this hypothesis. Moreover, our data show that in vitro dipyridamole treatment for 4 h inhibits Wnt and ERK1/2-MAPK pathways, but does not impair the NF-kB pathway, which is then affected only 24 h later during the treatment. This could lead to the hypothesis that inhibition of NF-kB is an indirect consequence of the action of dipyridamole on the previous two affected pathways. Further studies performed with specific inhibitors of these and other pathways are needed to address this question, thus dissecting further the mechanism of dipyridamole action.

Another molecular mechanism, by which dipyridamole might exert its in vivo therapeutic effects is through the impairment of TAM and MDSC infiltration. Within the tumor microenvironment, both TAMs and MDSCs have pro-tumoral functions, which thus promote tumor-cell survival and proliferation, along with angiogenesis, incessant matrix turnover, dissemination and repression of adaptive immunity [52, 53]. Therefore, attenuation of the infiltration of these immune cells might result in reductions in tumor growth and invasiveness.

Biochemical studies have also identified the transcription factor NF-kB as a master regulator of cancer-related

inflammation in TAMs and in neoplastic cells. Constitutive NF-kB activation is indeed often seen in cancer cells, and this might be promoted by cytokines (e.g., IL-1β and TNFα) expressed by TAMs or other stromal cells, as well as by environmental cues (e.g., hypoxia and reactive oxygen intermediates) or by genetic alterations [54]. NF-kB induces several cellular modifications associated with tumorigenesis and with more aggressive phenotypes, which include self-sufficiency in growth signals, insensitivity to growth inhibition, resistance to apoptotic signals, angiogenesis, and cell migration and tissue invasion [55]. Therefore, this ability for dipyridamole to affect the tumor microenvironment might be due to its inhibitory effects on the NF-kB signaling pathway. Moreover, given the dipyridamole ability to impair cell motility, we could not rule out the possibility that the reduced infiltration of immune cells in the tumor microenvironment might be ascribed not only to its inhibitory effects on the NF-kB signaling pathway but also to its putative effect on the motility of these cells. Further studies will be needed to address this question.

In conclusion, the present study provides further insights into the molecular mechanisms of dipyridamole action, showing its ability to inhibit triple-negative breast-cancer primary tumor growth and metastasis formation. Moreover, our data document the ability of dipyridamole to decrease the activation of the Wnt, ERK1/2-MAPK and NF-kB signaling pathways. Finally, we have also described new biological functions of dipyridamole, showing its attenuation of immune inflammatory cell infiltration, which thus interferes with metastatic niche formation. We suggest that with appropriate doses and the correct mode of administration, dipyridamole is a promising agent for prevention of triple-negative primary and metastatic breast cancer, thus already also implying its potential use in other cancers that show highly activated Wnt, ERK1/2-MAPK and NF-kB signaling pathways.

Acknowledgments We would like to thank: Prof. Eugene Lukanidin for sharing the S100A4 antibodies used in this study, Prof. Luigi del Vecchio and Dr. Maddalena Raia for technical advice with the FACS analyses, Dr. Donatella Montanaro for technical advice with histological analyses, and Prof. Francesco Salvatore for supporting the project with the instrumentation required for in vivo imaging in mice. We also thank Viviana Vastolo for technical assistance in in vivo experiments. Associazione Italiana per la ricerca sul Cancro AIRC (MZ), Associazione Italiana per la lotta al Neuroblastoma (MZ). This study was also supported in part by the Intramural Research Program of the National Cancer Institute (PSS). DS was supported by the Dipartimento di Biochimica e Biotecnologie Mediche, 'Federico II' University of Naples; VDD was supported by the Fondazione San Paolo (IM) and Tumic; DMD was supported by a Dottorato in Medicina Molecolare, 'Federico II' University of Naples; GDV was supported by a Dottorato in Medicina Molecolare, 'Federico II' University of Naples; and CM was supported by a Dottorato in Produzione e Sanità degli Alimenti di Origine Animale, 'Federico II' University of Naples.

Conflict of interest The authors declare that they have no competing interests as defined by Clinical & Experimental Metastasis, or other interests that might be perceived as influencing the results and discussion reported in this manuscript.

References

1. Jemal A, Bray F, Center MM, Ferlay J, Ward E, Forman D (2011) Global cancer statistics. CA Cancer J Clin 61:69–90
2. Steeg PS (2006) Tumor metastasis: mechanistic insights and clinical challenges. Nat Med 12:895–904
3. Schaper W (2005) Dipyridamole, an underestimated vascular protective drug. Cardiovasc Drugs Ther 19:357–363
4. Belt JA, Marina NM, Phelps DA, Crawford CR (1993) Nucleoside transport in normal and neoplastic cells. Adv Enzyme Regul 33:235–252
5. Walling J (2006) From methotrexate to pemetrexed and beyond. A review of the pharmacodynamic and clinical properties of antifolates. Invest New Drugs 24:37–77
6. Howell SB, Hom D, Sanga R, Vick JS, Abramson IS (1989) Comparison of the synergistic potentiation of etoposide, doxorubicin, and vinblastine cytotoxicity by dipyridamole. Cancer Res 49:3178–3183
7. Ramu N, Ramu A (1989) Circumvention of adriamycin resistance by dipyridamole analogues: a structure-activity relationship study. Int J Cancer 43:487–491
8. Lehman NL, Danenberg PV (2000) Modulation of RTX cytotoxicity by thymidine and dipyridamole in vitro: implications for chemotherapy. Cancer Chemother Pharmacol 45:142–148
9. Nelson JA, Drake S (1984) Potentiation of methotrexate toxicity by dipyridamole. Cancer Res 44:2493–2496
10. Desai PB, Sridhar R (1992) Potentiation of cytotoxicity of mitoxantrone toward CHO-K1 cells in vitro by dipyridamole. Pharm Res 9:178–181
11. Boyer CR, Karjian PL, Wahl GM, Pegram M, Neuteboom ST (2002) Nucleoside transport inhibitors, dipyridamole and p-nitrobenzylthioinosine, selectively potentiate the antitumor activity of NB1011. Anticancer Drugs 13:29–36
12. Rodrigues M, Barbosa F Jr, Perussi JR (2004) Dipyridamole increases the cytotoxicity of cisplatin in human larynx cancer cells in vitro. Braz J Med Biol Res 37:591–599
13. Sato S, Kohno K, Hidaka K, Hisatsugu T, Kuwano M, Komiyama S (1993) Differentially potentiating effects by dipyridamole on cytotoxicity of 5-fluorouracil against three human maxillary cancer cell lines derived from a single tumor. Anticancer Drug Des 8:289–297
14. Kennedy DG, Van den Berg HW, Clarke R, Murphy RF (1986) Enhancement of methotrexate cytotoxicity towards the MDA.MB.436 human breast cancer cell line by dipyridamole. The role of methotrexate polyglutamates. Biochem Pharmacol 35:3053–3056
15. Goda AE, Yoshida T, Horinaka M, Yasuda T, Shiraishi T, Wakada M, Sakai T (2008) Mechanisms of enhancement of TRAIL tumoricidal activity against human cancer cells of different origin by dipyridamole. Oncogene 27:3435–3445
16. Zhang Y, Gupta A, Wang H, Zhou L, Vethanayagam RR, Unadkat JD, Mao Q (2005) BCRP transports dipyridamole and is inhibited by calcium channel blockers. Pharm Res 22:2023–2034
17. Haimeur A, Conseil G, Deeley RG, Cole SP (2004) The MRP-related and BCRP/ABCG2 multidrug resistance proteins: biology, substrate specificity and regulation. Curr Drug Metab 5:21–53

18. Eisert WG (2002) Dipyridamole. In: Michelson AD (ed) Platelets. Academic Press, Amsterdam, pp 803–815
19. White H, Jamieson DG (2010) Review of the ESPRIT Study: aspirin plus dipyridamole versus aspirin alone for prevention of vascular events after a noncardioembolic, mild-to-moderate ischemic stroke or transient ischemic attack. Postgrad Med 122:227–229
20. Tsuruo T, Fujita N (2008) Platelet aggregation in the formation of tumor metastasis. Proc Jpn Acad Ser B Phys Biol Sci 84: 189–198
21. Nierodzik ML, Karpatkin S (2006) Thrombin induces tumor growth, metastasis, and angiogenesis: evidence for a thrombin-regulated dormant tumor phenotype. Cancer Cell 10:355–362
22. Isacoff WH, Bendetti JK, Barstis JJ, Jazieh AR, Macdonald JS, Philip PA (2007) Phase II trial of infusional fluorouracil, leucovorin, mitomycin, and dipyridamole in locally advanced unresectable pancreatic adenocarcinoma: SWOG S9700. J Clin Oncol 25:1665–1669
23. Raschko JW, Synold TW, Chow W, Coluzzi P, Hamasaki V, Leong LA, Margolin KA, Morgan RJ, Shibata SI, Somlo G, Tetef ML, Yen Y, ter Veer A, Doroshow JH (2000) A phase I study of carboplatin and etoposide administered in conjunction with dipyridamole, prochlorperazine and cyclosporine A. Cancer Chemother Pharmacol 46:403–410
24. Burch PA, Ghosh C, Schroeder G, Allmer C, Woodhouse CL, Goldberg RM, Addo F, Bernath AM, Tschetter LK, Windschitl HE, Cobau CD (2000) Phase II evaluation of continuous-infusion 5-fluorouracil, leucovorin, mitomycin-C, and oral dipyridamole in advanced measurable pancreatic cancer: a North Central Cancer Treatment Group Trial. Am J Clin Oncol 23:534–537
25. Wenzel J, Zeisig R, Fichtner I (2009) Inhibition of breast cancer metastasis by dual liposomes to disturb complex formation. Int J Pharm 370:121–128
26. Wenzel J, Zeisig R, Haider W, Habedank S, Fichtner I (2010) Inhibition of pulmonary metastasis in a human MT3 breast cancer xenograft model by dual liposomes preventing intravasal fibrin clot formation. Breast Cancer Res Treat 121:13–22
27. Foulkes WD, Smith IE, Reis-Filho JS (2010) Triple-negative breast cancer. N Engl J Med 363:1938–1948
28. Xing JZ, Zhu L, Gabos S, Xie L (2006) Microelectronic cell sensor assay for detection of cytotoxicity and prediction of acute toxicity. Toxicol in Vitro 20:995–1004
29. Spano D, Cimmino F, Capasso M, D'Angelo F, Zambrano N, Terracciano L, Iolascon A (2008) Changes of the hepatic proteome in hepatitis B-infected mouse model at early stages of fibrosis. J Proteome Res 7:2642–2653
30. Chuang KA, Lieu CH, Tsai WJ, Wu MH, Chen YC, Liao JF, Wang CC, Kuo YC (2010) Evaluation of anti-Wnt/β-catenin signaling agents by pGL4-TOP transfected stable cells with a luciferase reporter system. Braz J Med Biol Res 43:931–941
31. Vlad A, Röhrs S, Klein-Hitpass L, Müller O (2008) The first five years of the Wnt targetome. Cell Signal 20:795–802
32. Weyrich AS, Denis MM, Kuhlmann-Eyre JR, Spencer ED, Dixon DA, Marathe GK, McIntyre TM, Zimmerman GA, Prescott SM (2005) Dipyridamole selectively inhibits inflammatory gene expression in platelet-monocyte aggregates. Circulation 111:633–642
33. Chakrabarti S, Blair P, Wu C, Freedman JE (2007) Redox state of dipyridamole is a critical determinant for its beneficial antioxidant and antiinflammatory effects. J Cardiovasc Pharmacol 50:449–457
34. Sethi G, Ahn KS, Sung B, Aggarwal BB (2008) Pinitol targets nuclear factor-kappaB activation pathway leading to inhibition of gene products associated with proliferation, apoptosis, invasion, and angiogenesis. Mol Cancer Ther 7:1604–1614
35. Kawakami H, Tomita M, Matsuda T, Ohta T, Tanaka Y, Fujii M, Hatano M, Tokuhisa T, Mori N (2005) Transcriptional activation of survivin through the NF-kappaB pathway by human T-cell leukemia virus type I tax. Int J Cancer 115:967–974
36. Mantovani A (2010) Molecular pathways linking inflammation and cancer. Curr Mol Med 10:369–373
37. Boye K, Maelandsmo GM (2010) S100A4 and metastasis: a small actor playing many roles. Am J Pathol 176:528–535
38. Stein U, Arlt F, Walther W, Smith J, Waldman T, Harris ED, Mertins SD, Heizmann CW, Allard D, Birchmeier W, Schlag PM, Shoemaker RH (2006) The metastasis-associated gene S100A4 is a novel target of beta-catenin/T-cell factor signaling in colon cancer. Gastroenterology 131:1486–1500
39. Grotterød I, Maelandsmo GM, Boye K (2010) Signal transduction mechanisms involved in S100A4-induced activation of the transcription factor NF-kappaB. BMC Cancer 10:241
40. Haskó G, Kuhel DG, Chen JF, Schwarzschild MA, Deitch EA, Mabley JG, Marton A, Szabó C (2000) Adenosine inhibits IL-12 and TNF-[alpha] production via adenosine A2a receptor-dependent and independent mechanisms. FASEB J 14:2065–2074
41. Budd GT, Jayaraj A, Grabowski D, Adelstein D, Bauer L, Boyett J, Bukowski R, Murthy S, Weick J (1990) Phase I trial of dipyridamole with 5-fluorouracil and folinic acid. Cancer Res 50:7206–7211
42. Chakravarthy A, Abrams RA, Yeo CJ, Korman LT, Donehower RC, Hruban RH, Zahurek ML, Grochow LB, O'Reilly S, Hurwitz H, Jaffee EM, Lillemoe KD, Cameron JL (2000) Intensified adjuvant combined modality therapy for resected periampullary adenocarcinoma: acceptable toxicity and suggestion of improved 1-year disease-free survival. Int J Radiat Oncol Biol Phys 48:1089–1096
43. Willson JK, Fischer PH, Tutsch K, Alberti D, Simon K, Hamilton RD, Bruggink J, Koeller JM, Tormey DC, Earhart RH, Ranhosky A, Trump DL (1988) Phase I clinical trial of a combination of dipyridamole and acivicin based upon inhibition of nucleoside salvage. Cancer Res 48:5585–5590
44. Goel R, Cleary SM, Horton C, Balis FM, Zimm S, Kirmani S, Howell SB (1989) Selective intraperitoneal biochemical modulation of methotrexate by dipyridamole. J Clin Oncol 7:262–269
45. Isonishi S, Kirmani S, Kim S, Plaxe SC, Braly PS, McClay EF, Howell SB (1991) Phase I and pharmacokinetic trial of intraperitoneal etoposide in combination with the multidrug-resistance-modulating agent dipyridamole. J Natl Cancer Inst 83:621–626
46. Mahony C, Wolfram KM, Cocchetto DM, Bjornsson TD (1982) Dipyridamol kinetics. Clin Pharmacol Ther 31:330–338
47. Curtin NJ, Bowman KJ, Turner RN, Huang B, Loughlin PJ, Calvert AH, Golding BT, Griffin RJ, Newell DR (1999) Potentiation of the cytotoxicity of thymidylate synthase (TS) inhibitors by dipyridamole analogues with reduced alpha1-acid glycoprotein binding. Br J Cancer 80:1738–1746
48. Huang C, Jacobson K, Schaller MD (2004) MAP kinases and cell migration. J Cell Sci 117:4619–4628
49. Kaler P, Godasi BN, Augenlicht L, Klampfer L (2009) The NF-kappaB/AKT-dependent Induction of Wnt Signaling in Colon Cancer Cells by Macrophages and IL-1beta. Cancer Microenviron 2:69–80
50. Kim D, Rath O, Kolch W, Cho KH (2007) A hidden oncogenic positive feedback loop caused by crosstalk between Wnt and ERK pathways. Oncogene 26:4571–4579
51. Chuderland D, Seger R (2005) Protein-protein interactions in the regulation of the extracellular signal-regulated kinase. Mol Biotechnol 29:57–74
52. Solinas G, Germano G, Mantovani A, Allavena P (2009) Tumor-associated macrophages (TAM) as major players of the cancer-related inflammation. J Leukoc Biol 86:1065–1073

53. Hanahan D, Weinberg RA (2011) Hallmarks of cancer: the next generation. Cell 144:646–674
54. Karin M (2006) Nuclear factor-kappaB in cancer development and progression. Nature 441:431–436
55. Pikarsky E, Porat RM, Stein I, Abramovitch R, Amit S, Kasem S, Gutkovich-Pyest E, Urieli-Shoval S, Galun E, Ben-Neriah Y (2004) NF-kappaB functions as a tumour promoter in inflammation-associated cancer. Nature 431:461–466